Summer 2022

Structural and Functional Characterization of Two Poly(aspartic acid) Hydrolases

Amanda Jansch

STRUCTURAL AND FUNCTIONAL CHARACTERIZATION OF TWO POLY(ASPARTIC ACID) HYDROLASES

by

AMANDA JANSCH

(Under the Direction of Mitch Weiland)

ABSTRACT

Due to the accumulation of polymers in the environment, biodegradable alternatives should be used in place of commonly used polymers like poly(carboxylates). Poly(carboxylates) are water-soluble polymers (WSPs) that make up a variety of consumer products, such as detergents, descaling agents, and superabsorbent materials commonly found in diapers and feminine hygiene products. While the visible accumulation of these products may not be obvious, it is necessary to reduce the amount entering the environment. Poly(aspartic acid) (PAA) is an alternative WSP that is biodegradable through the action of three different enzymes, $PahZ1_{KT-1}$, $PahZ2_{KT-1}$, and $PahZ1_{KP-2}$. Originally isolated from river water bacteria strains *Sphingomonas* sp. KT-1 and *Pedobactor* sp. KP-2, these enzymes were reported to break down poly(aspartic acid) to the original monomer, aspartic acid. $PahZ1_{KT-1}$, a serine protease, cleaves β-amide linkages to form oligo(aspartic acid) (OAA), which is then acted upon by $PahZ2_{KT-1}$. $PahZ2_{KT-1}$ acts upon both α- and β- amide linkages, forming monomeric aspartic acid as a product, and requires the presence of zinc ions in the active site for catalytic activity. $PahZ1_{KP-2}$, a $PahZ1_{KT-1}$ homolog, is a putative serine protease that cleaves high-molecular weight PAA at the β-amide linkage. This thesis focuses on the characterization of these needed poly(aspartic acid) degrading enzymes through elucidation of their crystal structures and important residues for catalytic activity and substrate binding. Structural and functional knowledge of each enzyme will allow for protein engineering to enhance poly(aspartic acid) degradation and future degradation of other WSPs.

INDEX WORDS: PahZ1, PahZ2, Poly(aspartic acid), Serine protease, Metalloprotease, Poly(aspartic acid) hydrolase, *Sphingomonas* sp. KT-1, *Pedobactor* sp. KP-2, GPC chromatography

STRUCTURAL AND FUNCTIONAL CHARACTERIZATION OF TWO POLY(ASPARTIC ACID) HYDROLASES

by

AMANDA JANSCH

B.S., Georgia Southern University, 2021

A Thesis Submitted to the Graduate Faculty of Georgia Southern University

in Partial Fulfillment of the Requirements for the Degree

MASTER OF SCIENCE

STRUCTURAL AND FUNCTIONAL CHARACTERIZATION OF TWO POLY(ASPARTIC ACID) HYDROLASES

by

AMANDA JANSCH

Major Professor:	Mitch Weiland
Committee:	Nathaniel Shank
	Beverly Penland

Electronic Version Approved:
July 2022

ACKNOWLEDGMENTS

I would like to thank Dr. Weiland for all that he has done to help me succeed over the last five years. Thank you to my thesis committee, Dr. Shank and Dr. Penland, for their time, feedback, and guidance as I prepared my thesis.

I would also like to acknowledge the following for all of their time and support:

Tarah Yared for all of the support with PAAH-2 in the lab as well as outside of the lab.

Dr. Groom for the infinite amount of time and knowledge he was willing to share.

Dr. McGibony for all of her guidance through the graduate program.

Many of the graduate students for their constant support as we succeeded together.

TABLE OF CONTENTS

Page

LIST OF TABLES

Page

LIST OF FIGURES

Page

CHAPTER 1

INTRODUCTION

1.1 Accumulation of Polymers in the Environment

Plastic products are present throughout society, taking the form of containers, toys, material coatings, packaging products, and countless other consumer goods. These products, made up of synthetic polymers, have a lasting effect in the environment. While recycling can help decrease environmental accumulation, many products are not properly disposed of and end up damaging ecological systems as their buildup in the environment increases.[1] Over the last ten years, there has been a significant push for manufacturers and consumers to shift from single-use plastics to biodegradable or reusable alternatives. This push comes from the visible accumulation of synthetic polymers, as more than 80% of these products end up in landfills.[2] These synthetic polymers can be divided into two different classes: 1) water-insoluble polymers (WIPs), and 2) water-soluble polymers (WSPs).[3, 4] From a media perspective, WIPs tend to gain most of the attention, as their accumulation in the environment is evident by the many landfills that exist all over the world. Poly(ethylene terephthalate) (PET), one of the most abundant synthetic WIPs used in the plastic industry, is most often used to make beverage containers that hold products like water or soda.[5] To mitigate PET accumulation, scientists are working to enhance the catalytic activity of a PET degrading enzyme, PETase.[6] While these WIPs are gaining attention due to their visible accumulation, there should also be concern about the unseen, water-soluble polymers (WSPs) accumulating in the environment.[3, 4]

WSPs are used in a variety of everyday products, from detergents and pharmaceuticals to superabsorbent materials found in diapers and feminine hygiene products.[3] While their applications seem limitless, so are their environmental lifetimes because many of the commonly used WSPs are resistant to breakdown and biodegradation.[7] The more commonly used WSPs, such as poly(acrylamides) and poly(carboxylates), are not a threat to human health in their polymer form, but may break down in the environment to form products that are harmful.[7, 8] For example, poly(acrylamide), commonly used as a

water flocculent in waste-water treatment, can undergo thermal degradation in the environment to form the neurotoxin acrylamide. While poly(acrylamide) is not a reported threat to the environment, its monomer acrylamide can damage ecosystems and negatively impact aquatic life.[9, 10] Poly(carboxylates) are a threat as well, and appear in a variety of household products like detergents and anti-scaling agents. Studies have shown that the polymer is persistent, and often present in soil and waste-water sludge with little to no biodegradation over time.[11] Therefore, there is a need to reduce the environmental accumulation of these products before they pose the same issues seen with WIPs.

1.2 Poly(aspartic acid): Uses and Importance

To mitigate the environmental accumulation of WSPs, biodegradable alternatives are necessary. Poly(aspartic acid) (PAA), is an alternative for poly(carboxylates), but unlike poly(carboxylates), PAA is biodegradable and environmentally friendly.[12] The biodegradable polymer can be thermally synthesized from naturally occurring aspartic acid, forming α- and β-linked thermally synthesized poly(aspartic acid) (tPAA) shown in Figure 1. Synthesis of tPAA starts by heating L-aspartic acid to form a poly(succinimide) (PSI) intermediate, which then undergoes ring-opening hydrolysis in the presence of NaOH and heat to form α- and β-linked tPAA.[13] When thermally synthesized, tPAA has unique properties as it forms about 70% of the β-amide linkage and only 30% of the α-amide. The polymer also tends to have branched units and irregular end groups that may influence the biodegradability of tPAA.[14, 15] These irregular end

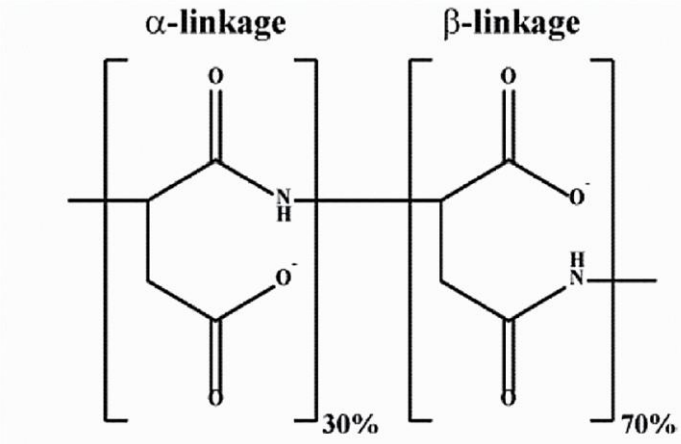

Figure 1. Representative α- and β-linked poly(aspartic acid) substrate. The frequency of each when thermally synthesized is provided as a percentage. Figure is reprinted with permission from Brambley, C. A.; Bolay, A. L.; Salvo, H.; Jansch, A. L.; Yared, T. J.; Miller, J. M.; Wallen, J. R.; Weiland, M. H., Structural Characterization of Sphingomonas sp. KT-1 PahZ1-Catalyzed Biodegradation of Thermally Synthesized Poly(aspartic acid). *ACS Sustainable Chemistry & Engineering* **2020,** *8* (29), 10702-10713. Copyright 2020 American Chemical Society.

groups are present due to side reactions that occur during the hydrolysis of PSI, forming a maleimide, fumaramide, fumaramic acid, dicarboxylic acid, or succinimide end group.[15]

Currently poly(carboxylates) undergo a cradle-to-grave process, meaning after synthesis and use the product will be disposed of. With tPAA, the ideal scenario is to start with naturally occurring aspartic acid, create the functional tPAA product, and then completely breakdown the tPAA to form the original starting material, aspartic acid. This process is referred to as cradle-to-cradle, and is a conceivable scenario through the action of the three enzymes identified as poly(aspartic acid) hydrolases.

1.3 Enzymes Capable of Poly(aspartic acid) Degradation

The biodegradation of tPAA was first identified in two river water bacteria strains, *Sphingomonas sp.* KT-1 and *Pedobactor sp.* KP-2.[14, 16] Initial incubation studies with *Sphingomonas sp.* KT-1 showed an inability to break down PAA larger than 5 kDa, while incubation studies with *Pedobactor sp.* KP-2 resulted in the breakdown of high-molecular weight PAA (5-150 kDa) to produce products 250 to 5,000 Da in size. When the *Sphingomonas* and *Pedobactor* strains were mixed and incubated with high-molecular weight tPAA, one of the products generated was monomeric aspartic acid.[14] Later studies of the strains led to the initial isolation and characterization of three different poly(aspartic acid) hydrolases: $PahZ1_{KT-1}$, $PahZ2_{KT-1}$, and $PahZ1_{KP-2}$.[14]

Initial purification studies of $PahZ1_{KT-1}$ identified an enzyme with a molecular weight of approximately 30 kDa, while inhibitory studies using diisopropyl fluorophosphates (DFP) and phenylmethylsulfonyl fluoride (PMSF) suggested the enzyme is a serine protease, which was later supported by a loss of activity when the serine at the catalytic site was replaced with an alanine.[14, 17] NMR studies identified that $PahZ1_{KT-1}$ cleavage of low-molecular weight tPAA occurred in an endolytic manner at the β-amide, forming oligomeric aspartic acid (OAA) as its product.[14, 17] Initial characterization studies also identified the $PahZ1_{KT-1}$ catalytic site as similar to the catalytic domain of poly(hydroxybutyrate) (PHB), which suggests an evolutionary connection due to the overlapping amino acid sequence between the catalytic sites.[14]

After the initial characterization of PahZ1$_{KT-1}$, PahZ2$_{KT-1}$ was identified as the second enzyme from the *Sphingomonas* strain. Results showed PahZ1$_{KT-1}$ first acted upon the low molecular weight tPAA at the β-linkage in an endolytic manner, forming OAA, and PahZ2$_{KT-1}$ cleaved both α- or β-linked OAA to form monomeric aspartic acid.[14, 18] Characterization studies of PahZ2$_{KT-1}$ found similarities in the amino acid sequence to a putative metallopeptidase CB15 from *Caulobacter crescentus*, which suggested the necessity for a metal ion within the active site of PahZ2$_{KT-1}$.[14]

PahZ1$_{KP-2}$ from the *Pedobactor* strain, identified as a homolog of PahZ1$_{KT-1}$, was the third enzyme capable of PAA degradation. PahZ1$_{KP-2}$ was also recognized as a potential serine protease that cleaves high and low molecular weight PAA in an endolytic manner at the β-amide.

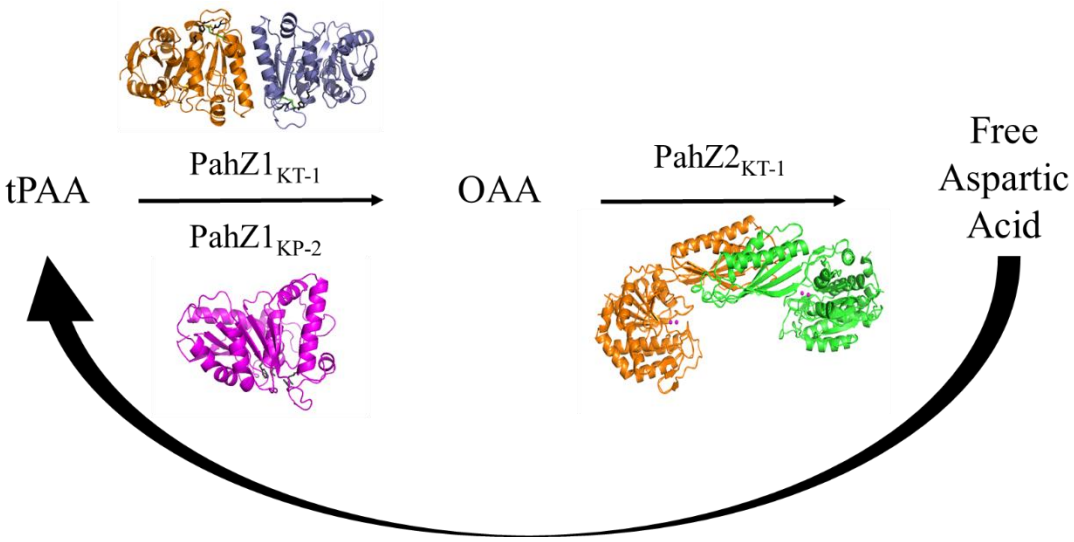

Figure 2. Cradle-to-cradle process of tPAA degradation. PahZ1$_{KT-1}$ or PahZ1$_{KP-2}$ break down thermally synthesized poly(aspartic acid) (tPAA) to oligomeric aspartic acid (OAA), which is then acted upon by PahZ2$_{KT-1}$ to form monomeric aspartic acid. The structure of PahZ1$_{KT-1}$ is shown in orange and slate, while the structure of PahZ1$_{KP-2}$ is shown in magenta. The structure of PahZ2$_{KT-1}$ is shown in orange and green.

While these enzymes were initially characterized, there was no structure or mechanism studies available to facilitate a complete understanding of the cradle-to-cradle process outlined in Figure 2. Identifying the structure of each enzyme will further our understanding of how each enzyme functions, as

well as assist with identifying residue important to catalytic activity or substrate binding. Furthermore, characterization would assist with further engineering as we work towards the development of efficient enzymes that can break down other WSPs.

CHAPTER 2

CHARACTERIZATION OF PAHZ1$_{KT-1}$

2.1 Introduction to PahZ1$_{KT-1}$

PahZ1 was first isolated from the river water bacterial strain, *Sphingomonas* sp. KT-1 and identified as an endolytic PAA degrading enzyme capable of cleaving PAA with a molecular weight less than 5000 Da. PahZ1$_{KT-1}$ has specificity for cleavage at the β-amide and forms OAA that is used as the substrate for PahZ2$_{KT-1}$.[17] While results from initial studies[17] predicted that PahZ1$_{KT-1}$ was a serine protease, research efforts focused on the identification of the crystal structure, characterization of catalytic activity in regards to tPAA degradation, then identification and confirmation of the residues responsible for catalytic activity.

2.2 Methods

2.2.1 PahZ1$_{KT-1}$ Transformation, Expression and Purification

The gene for *PahZ1$_{KT-1}$*, consisting of 314 amino acids, was cloned in the pET15b vector with a 5' NdeI and 3' XhoI restriction site. The synthesis and cloning of the plasmid was performed by GenScript (Piscataway, NJ) and an N-terminus 6X histidine tag was included for purification. The plasmid was transformed into BL21 (DE3) *E. coli* cells according to the NEB protocol (New England Biolabs, Ipswich, MA) with the following exceptions: 250 uL of SOC was added, no serial dilutions were performed, and 25 uL and 250 uL of transformed cells were spread onto 1.5% LB Agar selection plates with carbenicillin to incubate. A well isolated colony was selected to inoculate a starter growth containing 50 mL of lysogeny broth (LB) media and 50 µg/mL carbenicillin. The starter growth incubated overnight at 37 ℃, shaking at 225 rpm, and was screened by purifying the plasmid according to the GeneJET Plasmid Miniprep Kit protocol (Thermo Scientific). PahZ1$_{KT-1}$ purified plasmid was incubated at 37 ℃ for 20 minutes with restriction endonucleases NdeI and XhoI for analysis using 1.2% Agarose gel electrophoresis.

Once screened for purity, 12.5 mL of the starter growth was used to inoculate 500 mL of LB-carb in 2L expression flasks. Cells were grown at 37 ℃, 225 rpm until the optical density ($O.D._{600}$) reached a range of 0.6 – 0.8. Once the ideal $O.D._{600}$ was reached, each flask was induced with 0.1 mM isopropyl β-D-1-thiogalactopyranoside (IPTG, GoldBio, St. Louis, MO) and transferred to an incubator at 20 ℃, 225 rpm overnight. Cells were harvested using centrifugation at 10,000 xg for 20 min at 4 ℃, and stored at -20 ℃.

The harvested cells were resuspended in start buffer (50 mM Tris, pH 8.0, 300 mM NaCl, and 20 mM imidazole), and lysed by sonication in an ice bath over a 45 min cycle with a 20 sec pulse, 59 sec rest, and 58% amplification. Following lysis, 125 units/mL of turbonuclease (Accelagen, San Diego, CA) and 10 µg/mL of lysozyme were added to enhance bacterial cell wall breakdown and remove genomic DNA. The cell lysate rocked for 60 min at room temperature before centrifugation at 10,000 xg for 20 min at 4 ℃ to pellet cell debris. The supernatant was loaded onto an AKTA FPLC with a HisPur Ni-nitriloacetic acid (NiNTA) column (Thermo Scientific, Waltham, MA) equilibrated in start buffer. The $PahZ1_{KT-1}$ protein was eluted from the NiNTA column using elution buffer (50 mM Tris, pH 8.0, 300 mM NaCl, 500 mM imidazole) over 60 min using a 0-100% gradient. Fractions of 3.0 mL were collected and run on a 12.5% SDS-PAGE at 150 V to analyze purity and identify the elution peak on the corresponding purification chromatogram. Identified fractions were collected and dialyzed in 20 mM Tris, pH 7.4, to get rid of any remaining imidazole. The purified protein was then stored on ice for characterization experiments.

2.2.2 GPC Activity Assays

To analyze the rate of substrate degradation, gel permeation chromatography (GPC) assays were performed with $PahZ1_{KT-1}$. The substrate, tPAA, was synthesized according to Andrzejak et al.[13], and 100 mg was solubilized in 1 mL of 50 mM potassium phosphate, pH 7.4, with 3 mg of internal standard, thyroglobulin (Millipore Sigma, Burlington, MA). Each sample contained 0.01 mg/mL of $PahZ1_{KT-1}$ and 24.5 µL of the substrate solution with a final sample volume of 100 µL. Samples were incubated at 37 ℃

over a period of 20 and 48 hrs, followed by heat precipitation of the protein at 80 ℃ for 10 mins. Samples were stored at -80 ℃ until loaded on the Shimadzu GPC.

To analyze degradation of the tPAA substrate over time, 10 µL of each sample was loaded onto a Shimadzu GPC with a Yarra 3 µM SEC-2000, 300 x 7.8 mm column (Phenomenex, Torrance, CA) equilibrated in 50 mM potassium phosphate, pH 7.4. Samples were detected by a refractive index detector, and the thyroglobulin was used as an internal standard to account for any differences in load amounts or chromatographic shifts. The common OAA product peak appeared at a retention time of 10.9 min, and a ratio of the product peak height compared to the internal standard height at a retention time of 5 min was used to calculate the total amount of tPAA degradation at each timepoint. The molecular weight of the OAA product peak at 10.9 min was determined using polyethylene glycol EasiVial GPC/SEC Calibration Standards (Agilent, Santa Clara, CA). A calibration curve was created with the LabSolutions GPC Software (Shimadzu), and the molecular weight for each integrated peak was calculated.

2.2.3 PahZ1$_{KT-1}$ Mutant Construct Analysis using GPC

The relative activity of PahZ1$_{KT-1}$ mutated constructs S157A, D225A, R246A, R246E, and R246K were determined by setting up a GPC assay using the same methods reported in the previous section (Section 2.2.2). The formation of product for each mutant was compared to the wild-type at a retention time of 10.9 min, in which the wild-type was set to 100%.

2.3 Results and Discussion

2.3.1 Crystal Structure of PahZ1$_{KT-1}$

Initial crystallization conditions were tested in 1,536 experiments at the Hauptman-Woodward Institute High-Throughput Crystallization Screening Center, and PahZ1$_{KT-1}$ crystallized in a number of conditions with some examples shown in Figure 3.

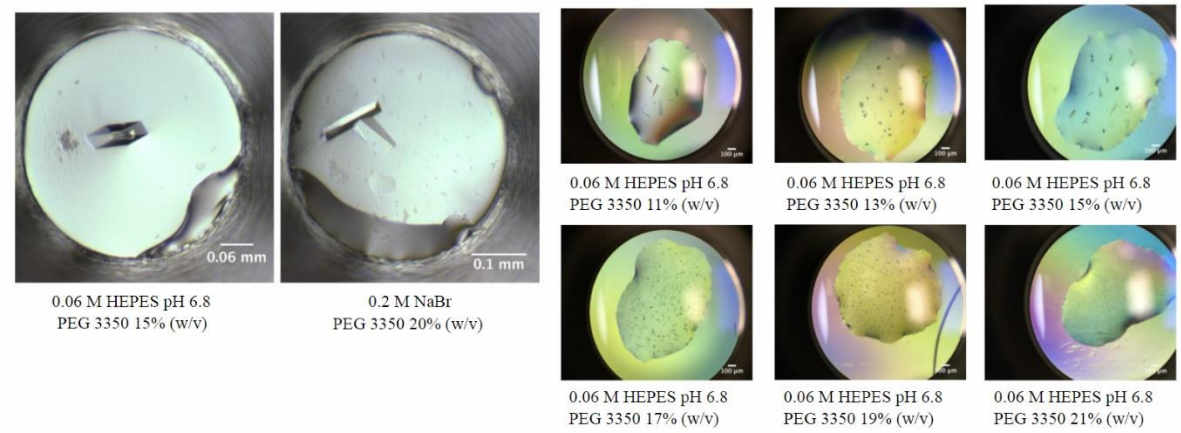

Figure 3. PahZ1$_{KT-1}$ initial crystallization experiments. The initial crystallization experiments showed large, single crystals in differing buffer solutions. These conditions were then pursued in-house to determine the crystal structure.

The conditions that gave large, single crystals were pursued by collaborator Dr. Wallen at Western Carolina University, and the structure was determined using molecular replacement, Figure 4A. The PahZ1$_{KT-1}$ structure is composed of two monomers in an asymmetric unit that form a dimer, with two-fold rotational symmetry at an α-helix made up of residues 244-265. An electrostatic map of the enzyme shows a positive trough, Figure 4B, leading toward the catalytic active site and is predicted to be necessary for substrate orientation.

PahZ1$_{KT-1}$ is a serine protease, and further analysis of the structure revealed the catalytic active site residues that were identified through molecular dynamic studies performed by Dr. Miller at Middle Tennessee State University. The active site of each monomeric unit is made up of a catalytic triad, residues S157, D225, and H280, Figure 4C. The catalytic active site cleaves poly(aspartic acid) using a typical serine protease mechanism, in which the nucleophilic serine will attack the carbonyl group of the substrate.[19] Based on molecular dynamics, hydrogen bonding occurs with residue R246, which may allow a D225-H280 interaction to improve the chance of a successful proton abstraction from S157 in the first step of the mechanism. Because of this, R246 was identified as a residue important for catalytic activity and further studied.

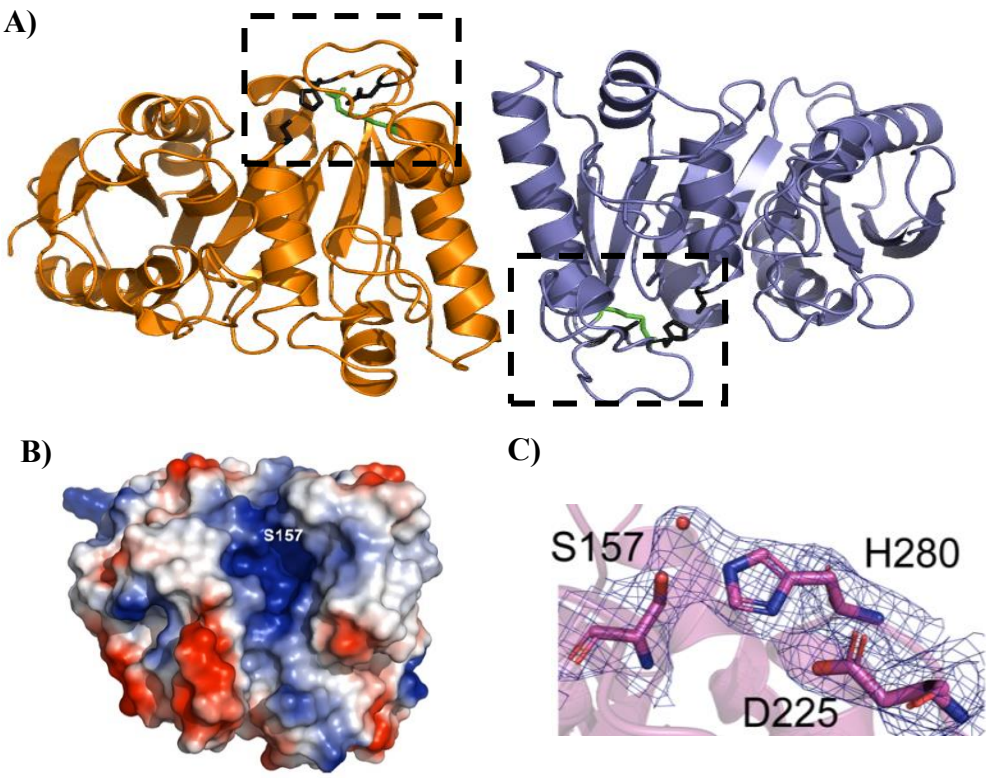

Figure 4. Crystal Structure of PahZ1$_{KT-1}$. A) Cartoon representation of the PahZ1$_{KT-1}$ crystal structure. The monomeric units are colored in orange and slate, with the catalytic active site (boxed region) residues highlighted in black. The R246 residue is highlighted in green. B) Electrostatic surface potential map of PahZ1$_{KT-1}$ with positively charged areas in blue, and negatively charged areas in red. The surface map shows a positive trough that leads to the catalytic active site, labeled with residue S157. C) A stick model of the active site residues in PahZ1$_{KT-1}$ that make up the catalytic triad of a typical serine protease. Figures B and C are reprinted with permission from Brambley, C. A.; Bolay, A. L.; Salvo, H.; Jansch, A. L.; Yared, T. J.; Miller, J. M.; Wallen, J. R.; Weiland, M. H., Structural Characterization of Sphingomonas sp. KT-1 PahZ1-Catalyzed Biodegradation of Thermally Synthesized Poly(aspartic acid). *ACS Sustainable Chemistry & Engineering* **2020,** *8* (29), 10702-10713. Copyright 2020 American Chemical Society.

2.3.2 GPC Activity Assay with Catalytic Site Mutants

To confirm the residues important for catalytic activity, GPC analysis was used to characterize the degradation of tPAA with mutated constructs D225A and S157A. The serine and aspartic acid were mutated to an alanine, an amino acid that is neutral, to inhibit any interaction of that residue with the substrate or other residues in the active site. The activity of each construct was compared to the wild-type by looking at the OAA product peak, and activity was greatly diminished when the mutations were introduced. Significant OAA product was formed with the wild-type after only 1 hr, whereas with the

mutated constructs the OAA product peak showed minimal product formation after 20 and 48 hrs of incubation, Figure 5. D225A had more activity than S157A, but after 48 hours the total OAA formed was 10% compared to the wild-type. S157A had almost no activity after 20 hours, and only about 3% OAA product formed after 48 hours. The significant decrease shows that residues S157 and D225 are necessary for catalytic activity, and supports the evidence that they make up the catalytic triad.

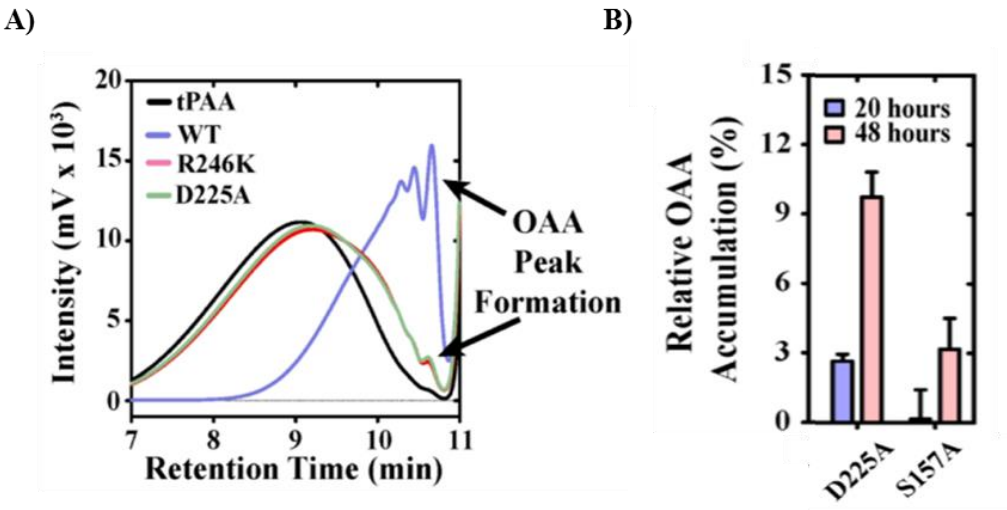

Figure 5. GPC activity of PahZ1$_{KT-1}$ catalytic mutants. A) An overlay of the chromatograms showing incubation with only tPAA (black), with PahZ1$_{KT-1}$ wild-type (slate), and D225A (green). The R246K mutant discussed later is also shown in red. An internal thyroglobulin standard, although not shown, is present at a retention time of 5 min. B) The OAA peak was analyzed at a retention time of 10.9 min and compared to the amount of product formed by the wild-type. Figures are reprinted with permission from Brambley, C. A.; Bolay, A. L.; Salvo, H.; Jansch, A. L.; Yared, T. J.; Miller, J. M.; Wallen, J. R.; Weiland, M. H., Structural Characterization of Sphingomonas sp. KT-1 PahZ1-Catalyzed Biodegradation of Thermally Synthesized Poly(aspartic acid). *ACS Sustainable Chemistry & Engineering* **2020,** *8* (29), 10702-10713. Copyright 2020 American Chemical Society.

While the amount of product formed was analyzed using a peak height comparison, the molecular weight of each product was calculated using a GPC calibration curve and the results are shown in Table 1. The M_n of the tPAA degraded by the wild-type at a retention time of 10.9 min was 2,983 g/mol, which is much smaller than the tPAA with no enzyme present, which had an M_n of 5,518 g/mol. The catalytic mutants, S157A and D225A showed a significant decrease activity and therefore had less OAA formed, as well as an M_n closer to that of the tPAA with no enzyme. While complete loss of catalytic activity was

not expected with S157A, there was still very little OAA formed and the M_n was comparable to tPAA with no enzyme present.

Table 1. $PahZ1_{KT-1}$ product molecular weight analysis. The polymer M_n and M_w values were determined from the corresponding chromatograms.

	tPAA	***Wild-Type***	***S157A***	***D225A***
M_n (g/mol)	5518	2983	5431	4920
M_w (g/mol)	7064	3294	7125	6490

2.3.3 Significance of Residue R246

Residue R246 was identified during molecular dynamic studies as important for catalytic activity, and may be the reason $PahZ1_{KT-1}$ has specificity for β-linked tPAA. In molecular dynamic studies, the interaction with the α- and β-carbonyl were studied with a focus on hydrogen bonding with residue R246. With the α-linked tPAA, the R246 residue has the ability to form multiple hydrogen bonds with the substrate, which changes the interactions between R246 and the catalytic active site. As seen in Figure 6A, R246 forms three hydrogen bonds with the substrate, which doesn't allow the substrate to then orient towards the catalytic active site. In Figure 6B, the α-linked tPAA forms an average of two hydrogen bonds with the protein itself which doesn't allow the substrate to then move towards the catalytic site. In Figure 6C, the substrate most often forms two hydrogen bonds with R246 specifically. The increased number of hydrogen bonding inhibits the movement of the α-linked substrate towards the catalytic active site for cleavage. With the β-linked tPAA, Figure 6A shows that there is little to no hydrogen bonding between the substrate and R246, and the residue instead swings toward the histidine in the catalytic active site. This allows the substrate to orient towards the active site, while R246 is likely stabilizing. Figures 6B and 6C show there are overall fewer interactions occurring with the β-linked substrate.

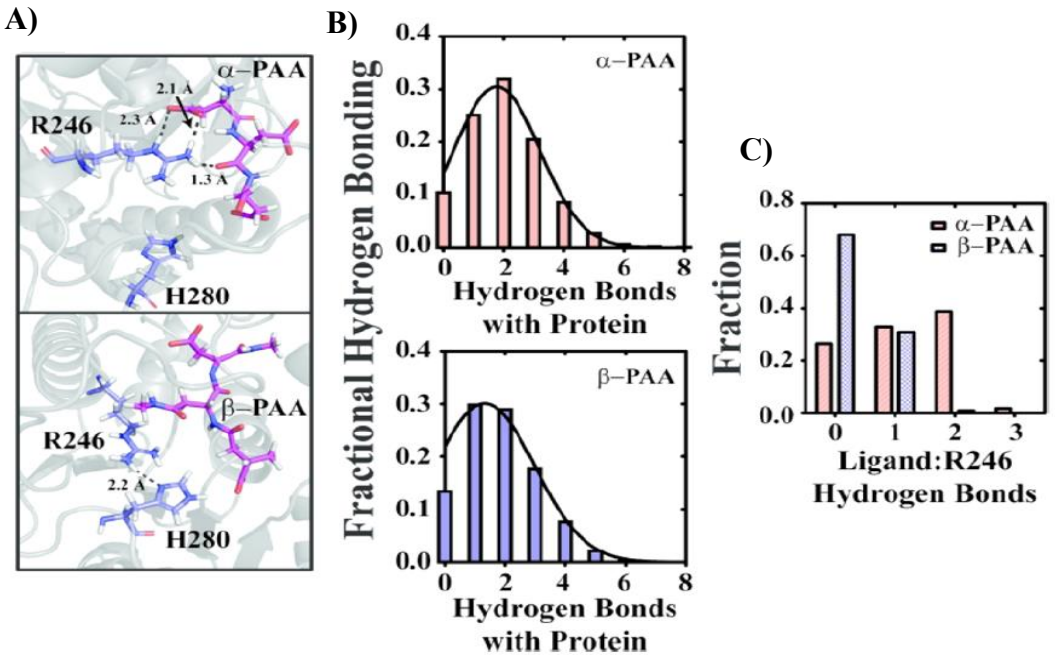

Figure 6. Comparison of the protein interactions with the α- and β-carbonyl. A) The position of the α-linked and β-linked PAA is studied in relationship to R246 and catalytic active site residue H280. B) The overall hydrogen bonding frequency between the protein and the substrate is shown, with β-linked PAA forming less hydrogen bonds with PahZ1$_{KT-1}$. C) Frequency of the hydrogen bonding between R246 and the substrate. The β-linked PAA often had little to no interaction with R246, while the α-linked PAA often formed one or two hydrogen bonds, and at times three hydrogen bonds. Figures are reprinted with permission from Brambley, C. A.; Bolay, A. L.; Salvo, H.; Jansch, A. L.; Yared, T. J.; Miller, J. M.; Wallen, J. R.; Weiland, M. H., Structural Characterization of Sphingomonas sp. KT-1 PahZ1-Catalyzed Biodegradation of Thermally Synthesized Poly(aspartic acid). *ACS Sustainable Chemistry & Engineering* **2020,** *8* (29), 10702-10713. Copyright 2020 American Chemical Society.

Using GPC analysis, the role of R246 was further assessed in regard to PAA degradation. Mutated constructs R246E, R246A, and R246K were created and compared to the wild-type in Figure 7. R246 mutations led to different product yields, as R246E had a complete loss of activity, while R246A and R246K had activity comparable to S157A and D225A. The complete loss of activity with R246E is predicted to be due to electrostatic repulsion of the polyanionic substrate. The data from the activity assay supports the prediction that R246 is involved with catalytic activity of PahZ1$_{KT-1}$ and necessary for stabilization.

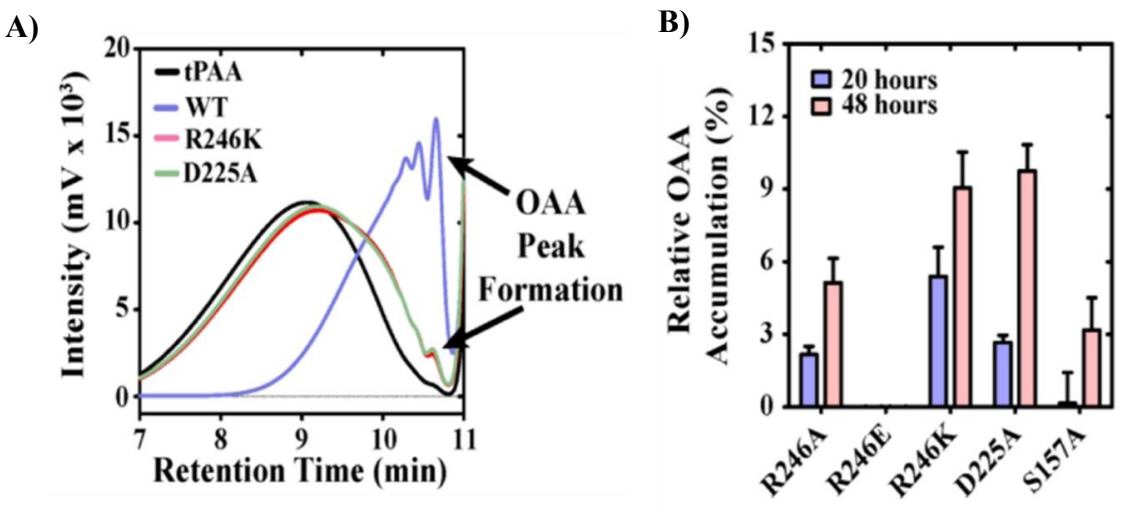

Figure 7. GPC activity analysis with R246 mutation. A) GPC chromatogram with the wild-type (slate) compared to construct R246K (red). B) Comparison of activity when residue R246 was mutated. The catalytic site constructs are included for comparison. Figures are reprinted with permission from Brambley, C. A.; Bolay, A. L.; Salvo, H.; Jansch, A. L.; Yared, T. J.; Miller, J. M.; Wallen, J. R.; Weiland, M. H., Structural Characterization of Sphingomonas sp. KT-1 PahZ1-Catalyzed Biodegradation of Thermally Synthesized Poly(aspartic acid). *ACS Sustainable Chemistry & Engineering* **2020,** *8* (29), 10702-10713. Copyright 2020 American Chemical Society.

2.4 Conclusion

PahZ1$_{KT-1}$ is a dimer made up of two monomeric units with two-fold rotational symmetry. There are hydrophobic interactions along the dimeric interface that stabilize the dimer, and a positive trough that binds the PAA and directs it to the catalytic active site. As a serine protease, the catalytic active site is made up of three amino acids; serine, aspartic acid, and histidine, identified as residues S157, D225, and H280. Molecular dynamic studies identified an arginine residue that provides rational for the specific cleavage of β-linked PAA. This residue, R246, was further confirmed as necessary for catalytic activity, along with residues S157 and D225 using GPC analysis after introducing point mutations at each site. Identification of the structure is important in further protein engineering studies to continue working towards creating an enzyme that can efficiently degrade water-soluble polymers.

CHAPTER 3

MONOMERIC CONSTRUCTS OF PAHZ1$_{KT-1}$

3.1 Introduction

3.1.1 E251K and IM PahZ1$_{KT-1}$ Monomer Design

After analysis of the wild-type PahZ1$_{KT-1}$ crystal structure, potential residues making up the dimeric interface were identified. It is predicted that anti-parallel α-helical strands present along the interface stabilize the symmetrical dimer, shown in Figure 8A. Residues R246 to H262 were identified from the X-ray structure as the residues that make up the anti-parallel α-helical strands. Previous studies[20] showed that when the nonpolar side chains making up the interface, specifically residue A255, were changed to a glutamate or tryptophan in silico, the free energy of dimerization was significantly reduced. Residue E251 was also identified as forming a hydrogen bond with H262, although in silico studies showed that there was not a reduction in free dimerization energy when E251 was mutated.[20] This information was important in the overall design of each monomeric construct. Further support that these residues were essential to dimerization came from the monomeric structure of PahZ1$_{KP-2}$, a PahZ1$_{KT-1}$ homolog.

For the first construct in Figure 8B, a single mutation at residue E251 was introduced to disrupt the hydrogen bond with H262. The glutamic acid at position 251 in the amino acid sequence was replaced with a lysine. This mutation from a negatively charged residue to a positively charged residue should not only disrupt the hydrogen bond that stabilizes the interface but also introduce repulsion. This construct is called E251K PahZ1$_{KT-1}$. The concern with E251K is that the nonpolar interface exposure could decrease the solubility of the protein, which led to the design and synthesis of a second monomeric construct.

The second construct in Figure 8C introduced more point mutations in an attempt to ensure that the protein solubility did not decrease as the nonpolar core of the interface was exposed. To determine which residues should be mutated, the sequence of the interface was compared to the similar sequence of a homologous protein that functions as a monomer.[21] There were four major differences

observed in the sequence at positions A248, E251, F252, and A255. These positions were mutated to mimic the hydrophilic homologous protein sequence, making up the construct IM (Interface Mutant). The mutations in this construct are A248E, E251K, F252T, and A255N. The mutations were introduced to disrupt the dimeric interphase without disrupting solubility.

The focus of this project was to confirm that the monomer of PahZ1$_{KT-1}$ had formed, and to then further assess the stability and activity of the monomeric constructs compared to PahZ1$_{KT-1}$ wild-type.

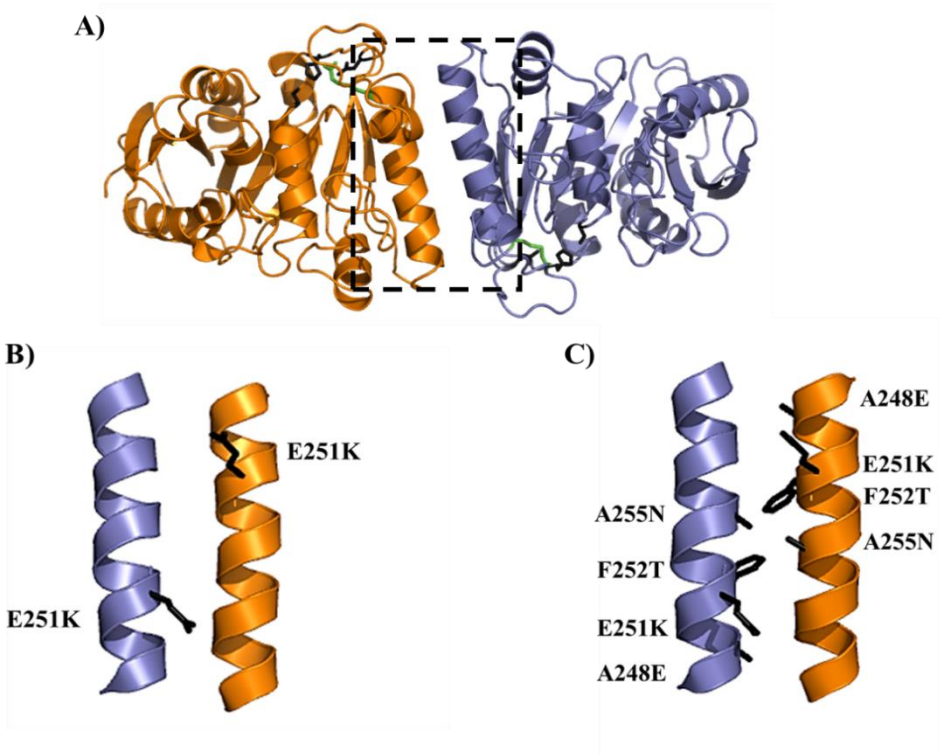

Figure 8. Representative structure of PahZ1$_{KT-1}$ highlighting interface mutations. A) The dimerization domain of PahZ1$_{KT-1}$ is highlighted by the black box. There are two alpha helices that interact, and constructs E251K and IM were made to disrupt the interactions between the two alpha helices. B) Construct E251K with the single point mutations labeled. C) Construct Interface Mutant (IM) with the four different mutations along each α-helix shown.

3.2 Methods

3.2.1 Transformation, Expression and Purification Methods

Synthesis of each construct was performed by GenScript (Piscataway, NJ) using the same pET15b vector as the PahZ1$_{KT-1}$ wild-type with a 5' NdeI and 3' XhoI restriction site. The transformation,

expression, and purification protocol was the same as previously reported with wild-type $PahZ1_{KT-1}$ (Chapter 2, Section 2.2.1).

3.2.2 Size Exclusion Chromatography

Each protein construct was run on a Sephacryl S200 Size Exclusion column attached to an AKTA purifier to determine if there was a size difference between the monomeric and dimeric constructs. Each sample loaded onto the column had a volume of 1.0 mL and contained 2.5 mg of protein. The column was equilibrated and run in 50 mM sodium phosphate, pH 7.4, at a flow rate of 0.5 mL/min. The protein was detected by UV absorption at λ=280 nm.

3.2.3 Protein Stability following Denaturation and Heat Precipitation

For analysis of protein refolding in the presence of guanidine hydrochloride (Gnd HCl) as a denaturant, each construct was brought to a concentration of 2.5 mg/mL with a volume of 1.0 mL. After, 6.0 M Gnd HCl was added until a final concentration of 2.5 M Gnd HCl was reached. Samples incubated at room temperature for 16 hours before exhaustively dialyzing against 50 mM HEPES, pH 7.4. Following dialysis, samples were centrifuged to pellet any precipitant and the supernatant was transferred into a new tube. The $O.D._{280}$ of the supernatant was read using a Nanodrop Lite Spectrophotometer (ThermoScientific) to determine the concentration of soluble protein remaining.

Protein stability was assessed by calculating recovery after heat denaturation. Assessment of protein refolding used the same volume and protein concentration as above, but samples were heated at 80 ℃ for 15 min to denature the enzyme. Samples were then centrifuged at 17,000 xg for 3 min to pellet any precipitated protein. The supernatant was transferred into a new tube and the $O.\ D._{280}$ was recorded and used to calculate the percent of protein precipitated. The pellet was resuspended in 0.5 mL of 6.0 M Gnd HCl to solubilize the protein, and vortexed until minimal precipitant remained. Each sample was then diluted to 2.5 M Gnd HCl final using 50 mM HEPES, pH 7.4. The $O.D._{280}$ of each sample was measured after resuspension and samples were brought to a final concentration of 1.2 mg/mL using 2.5 M Gnd HCl. Following dialysis against 50 mM HEPES, pH 7.4, samples were centrifuged to pellet any

remaining insoluble protein and the $O.D._{280}$ was measured to determine the final concentration of any soluble protein remaining.

3.2.4 Determination of Melting Temperature

To compare the thermal stability of the monomeric constructs to wild-type, the melting temperature of wild-type, E251K, and IM $PahZ1_{KT-1}$ was determined using an Agilent Cary 100 UV-VIS Spectrophotometer. All constructs were diluted to a final concentration of 0.2 mg/mL and added to a 500 µL quartz cuvette. Each run had a starting temperature of 20 ℃ and samples heated at a rate of 0.5 ℃/min until the temperature reached 95 ℃. Absorbance was detected at a wavelength of 280 nm. The point at which there was 50 % denaturation, the melting temperature, was determined by taking the first derivative of the melting curve.

3.2.5 Substrate Degradation Analysis using GPC

To determine how substrate degradation compared to the wild-type, each construct was analyzed using gel permeation chromatography (GPC). The first experiment was a timepoint assay, which looked at overall degradation over a period of time. The substrate, tPAA, was prepared by adding 100 mg of PAA to 1 mL of 50 mM HEPES pH 7.4. Each sample contained 24.5 mg PAA and 0.01 mg/mL enzyme with a final volume of 200 µL. While incubating at 37 ℃, 20 µL aliquots were collected at: 5 min, 15 min, 30 min, 1 hr, 2 hr, 3 hr, 4 hr. Each aliquot was then heated to 80 ℃ for 15 min using a heat block to precipitate the enzyme and stop any residual activity. Following heat denaturation, the aliquots were centrifuged at 17,000 xg for 1 min then stored at -80 ℃. The activity of each sample was determined using a Shimadzu GPC with a Yarra 3 µM SEC-2000, 300 x 7.8 mm column (Phenomenex, Torrance, CA) equilibrated in 50 mM HEPES pH 7.4 with a refractive index detector. Prior to injection, 10 µL of a 4.4 mg/mL stock of thyroglobulin (Millipore Sigma, Burlington, MA) was added to each aliquot to serve as an internal standard.

An activity assay was performed to determine if the protein constructs could refold properly and remain active after heat denaturation. Each sample was made following the same protocol as the time point assay, however, a 1 mL stock of each enzyme was first heated to 80 ℃ for 15 mins to precipitate the

protein, and then pelleted through centrifugation at 17,000xg for 3 mins. The supernatant was removed and the pelleted protein was resuspended in 1 mL of 2.5 M Guanidine HCl (Fisher Scientific, Fair Lawn, NJ) before exhaustively dialyzing against 50 mM HEPES pH 7.4 to remove all guanidine. Assay samples were made using the dialyzed refolded protein.

After heat denaturation, an assay was prepared to determine if PAA degradation occurred after each construct was unfolded using a denaturant and then refolded by dialyzing to remove the denaturant. To prepare the enzymes for the assay, 0.01 mg/mL of each construct was incubated at room temperature for 16 hrs with 2.5 M Guanidine HCl to denature the proteins. Each construct was placed in 50 mM HEPES, pH 7.4, to dialyze out the guanidine and promote refolding of the protein. The samples were prepared following the same protocol as the time point assay.

Analysis of substrate degradation was performed by comparing the height of a product peak at a retention time of 9.6 min to the height of the thyroglobulin internal standard at a retention time of 5.0 min. Once each product height was normalized using the internal standard height, the percent product formed was determined by subtracting the control from the product peak at each time point, which was then divided by the difference between the control and the wild-type at 4 hours. Wild-type at 4 hours with no treatment was set to 100%, and each construct was then compared to the wild-type with no treatment.

3.3 Results and Discussion

3.3.1 Confirmation of Dimeric Interface Disruption

During a previous study[20], the stability of the dimeric interface was assessed using a variety of techniques, including molecular modeling studies and size exclusion chromatography. Molecular modeling studies predicted that the amount of energy needed to disrupt the interface was equivalent to the

energy of two hydrogen bonds. The interaction is a nonpolar interaction, as the introduction of 150 mM and 500 mM NaCl did not disrupt the interface when injected on the size exclusion column, Figure 9.

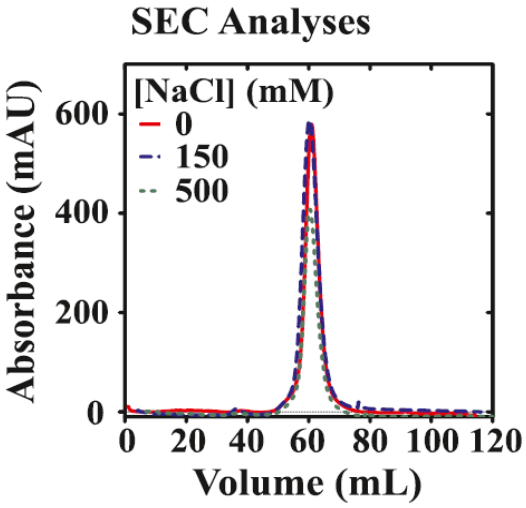

Figure 9. SEC chromatogram of PahZ1$_{KT-1}$ in the presence of NaCl. The experiments were performed with 0, 150, and 500 mM NaCl. Figures are reprinted with permission from Brambley, C. A.; Bolay, A. L.; Salvo, H.; Jansch, A. L.; Yared, T. J.; Miller, J. M.; Wallen, J. R.; Weiland, M. H., Structural Characterization of Sphingomonas sp. KT-1 PahZ1-Catalyzed Biodegradation of Thermally Synthesized Poly(aspartic acid). *ACS Sustainable Chemistry & Engineering* **2020,** *8* (29), 10702-10713. Copyright 2020 American Chemical Society.

With the mutated monomeric constructs, size-exclusion was used to confirm that the interface had been disrupted. With size exclusion chromatography (SEC), larger molecules will elute before smaller molecules. In this case, wild-type eluted first, at a volume of 58.3 mL. The smaller monomeric constructs eluted later, with E251K at 70.3 mL and IM at 70.0 mL. The monomeric constructs were expected to be around 32 kDa in size, while the wild-type was expected to twice the size at 64 kDa in size. The baseline resolution between the peaks in Figure 10A show that the wild-type is twice the size compared to the monomers. The similar elution time of the mutated constructs and the baseline resolution between peaks support the evidence that the mutations introduced did disrupt the dimeric interface. The chromatogram in Figure 10A shows the difference in elution times between the wild-type, E251K, and IM PahZ1$_{KT-1}$ constructs.

To further confirm that the dimeric interface was disrupted, dynamic light scattering (DLS) was used. DLS studies, Figure 10B, show a particle diameter difference between the wild-type and the monomeric constructs. In Figure 10B, the wild-type had a particle diameter close to 11 nm, while the IM and E251K had particle diameters closer to 7 nm. The peaks for the IM and E251K closely overlap, showing that they are very similar in size. Figure 10C shows the mean particle diameters based on replicate values. The estimated particle diameters for wild-type, E251K and IM are 9.0±1.0, 5.0±1.0, and

6.8±0.6 nm respectively. The mean particle diameters match the values predicted from the crystal structure of PahZ1$_{KT-1}$ wild-type. Based on SEC experiments as well as the DLS results, there is enough evidence to conclude that the mutations introduced in E251K and IM did disrupt the PahZ1$_{KT-1}$ wild-type dimer formation.

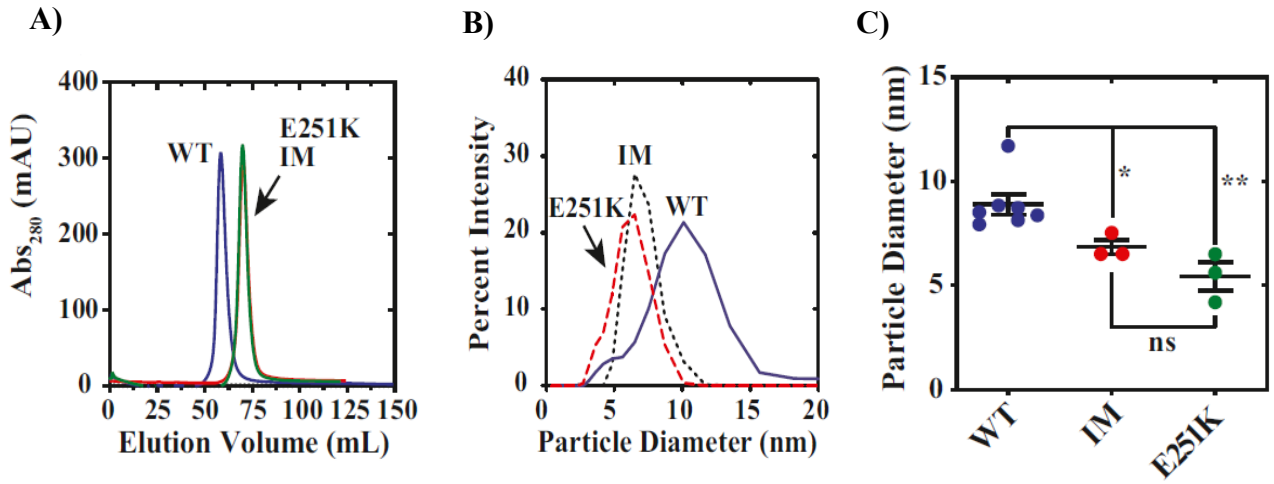

Figure 10. PahZ1$_{KT-1}$ particle diameter studies. A) SEC experiment with PahZ1$_{KT-1}$ WT, E251K and IM to show the size difference between dimeric and monomeric constructs. The wild-type is shown in blue, E251K in red, and IM in green. B) E251K and IM constructs are smaller than the dimeric wild-type in solution. E251K is represented as a red dashed line, IM as a blue dotted line, and wild-type as a blue solid line. B) The plot shows the fractional scattering intensity as a function of particle size. The esimate mean particle sizes are: wild-type 9±1 nm; E251K 5±1 nm; IM 6.8±0.6 nm. Figures are reprinted with permission from Lamantia, T.; Jansch, A.; Marsee, J. D.; Weiland, M. H.; Miller, J. M., Engineered Sphingomonas sp. KT-1 PahZ1 monomers efficiently degrade poly(aspartic acid). *Biophysical Chemistry* **2022,** *281*, 106745. Copyright 2022 Elsevier publishing.

3.3.2 Substrate Degradation Analysis Results

The normal activity assay assessed catalytic activity between the monomer and dimer. In this assay, each enzyme was incubated with the tPAA substrate and degradation was measured using GPC. Samples were removed from incubation and heat precipitated at different timepoints over a four hour period. Product formation was analyzed using the height at a retention time of 9.6 minutes, compared to the height of the internal thyroglobulin standard at 5.0 minutes. The amount of product formed by wild-type at four hours was set as 100% product formation, and the monomeric constructs were compared to the 100% product formation. As seen in Figure 11A, the catalytic activity of the monomeric constructs

did not change from the dimeric wild-type, and it was concluded that the ability of the enzyme to cleave tPAA was not dependent on its ability to dimerize.

Once it was determined that the catalytic activity of $PahZ1_{KT\text{-}1}$ did not change as a monomer, each construct was introduced to a stressor, either chemical denaturation or heat precipitation, in an attempt to mimic an industrial environment as increased stability and resilience could be important in commercial applications. In the post-heat treatment assay, the enzyme was heat precipitated, and the precipitated protein was resuspended in guanidine hydrochloride. After resuspension, each sample was exhaustively dialyzed to remove the denaturant and allow for refolding of the enzyme. Each enzyme was incubated with tPAA following the same protocol as the normal assay without stressors, and activity was analyzed. The results of this assay, in Figure 11B, show that E251K and IM are similar in activity with 99% and 98% activity respectively, however $PahZ1_{KT\text{-}1}$ wild-type activity decreased with only 93% activity retained after 240 minutes.

A similar result was seen with the wild-type in the post-unfolding assay. In this assay, each enzyme was incubated with a chemical denaturant, 2.5 M guanidine hydrochloride. After incubation with the denaturant, each enzyme was dialyzed exhaustively to completely remove the denaturant, and used in an assay following the same protocol as the normal assay. In Figure 11C, the relative activity of each construct is shown. While E251K and IM retain their activity, wild-type has a decrease in overall relative activity, retaining only 91% of its activity after incubating for 240 minutes. Overall, the thermal and chemical treatments did not have an effect on the activity of the monomeric constructs. The decreased maximum activity of $PahZ1_{KT\text{-}1}$ wild-type suggests an inability of the dimer to properly refold and retain catalytic activity, even when each construct is brought to identical enzyme concentrations prior to incubation with the substrate.

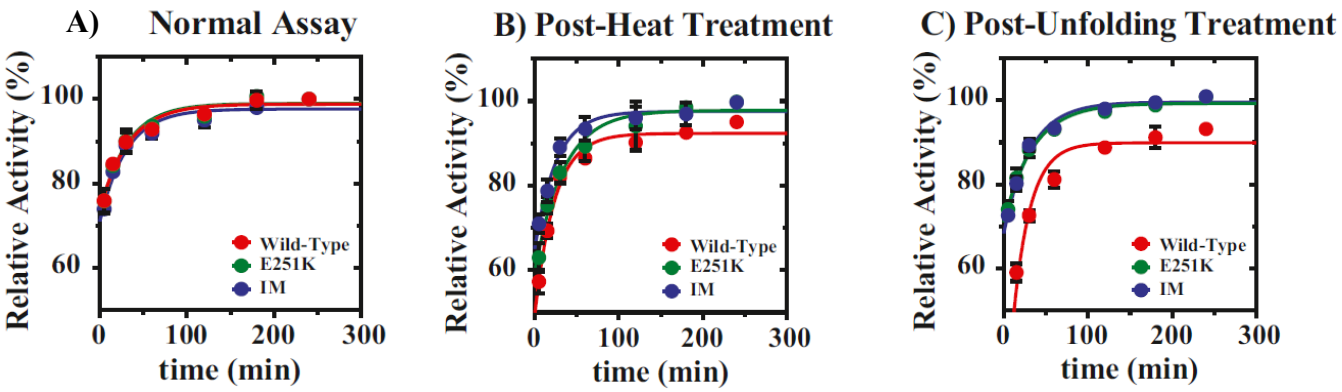

Figure 11. Relative catalytic activity of monomeric constructs compared to PahZ1$_{KT-1}$ using GPC analysis. A) PahZ1$_{KT-1}$ wild-type (red), E251K (green), and IM (blue) exhibit similar activity when degrading the tPAA substrate, with no difference in activity between the dimer and the monomer. B) After heat-treatment, where enzymes were precipitated and then refolded, PahZ1$_{KT-1}$ wild-type (red) shows a loss of catalytic activity compared to the monomeric constructs E251K (green) and IM (blue). C) After chemical denaturation and refolding, PahZ1$_{KT-1}$ wild-type (red) shows a loss of catalytic activity compared to constructs E251K (green) and IM (blue). Error bars represent the standard deviation of each timepoint. Figures are reprinted with permission from Lamantia, T.; Jansch, A.; Marsee, J. D.; Weiland, M. H.; Miller, J. M., Engineered Sphingomonas sp. KT-1 PahZ1 monomers efficiently degrade poly(aspartic acid). *Biophysical Chemistry* **2022,** *281*, 106745. Copyright 2022 Elsevier publishing.

3.3.3 Melting Temperature to Assess Stability

To further assess the stability of each construct, the melting temperatures were analyzed using UV-Vis spectroscopy. Each melting temperature, $T_{1/2}$, is indicated in Figure 12. The melting temperatures were determined by measuring the absorbance at 280 nm as the temperature increased from 25 ℃ to 95 ℃. The melting temperature was then calculated by taking the first derivative of the sigmoidal curve, and the single peak generated represented the melting temperature at which there was 50% denaturation. The starting absorbance represents the absorbance of the protein in its folded state, and as the temperature increased, the protein began to unfold and disrupt the transmittance of light, leading to an increase in absorbance. After heating to 95 ℃, each sample contained white precipitant, which indicated complete protein denaturation. As seen in Figure 12B, construct E251K had half the absorbance at the end compared to the other constructs due to scattering. There was less precipitant formed by E251K in the cuvette leading to a decreased absorbance compared to the constructs with quite a bit of precipitant formed. The melting temperatures of PahZ1$_{KT-1}$, E251K, and IM were 55.54±0.3 ℃, 56.8±0.3 ℃, and

56.7±0.7 ℃ respectively, indicating that the thermal stability is similar for dimeric and engineered monomeric constructs.

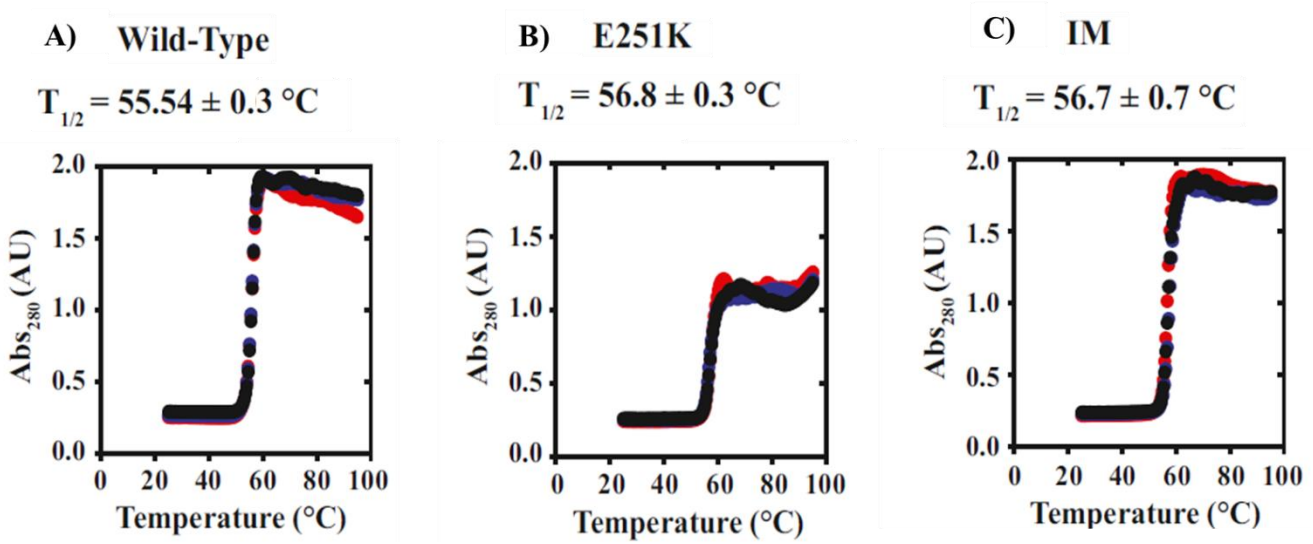

Figure 12. Average thermal stability between PahZ1$_{KT-1}$ constructs. Average melting temperatures of PahZ1$_{KT-1}$ (A), E251K (B), and IM (C) in solution. UV-vis spectroscopy measured the absorbance at 280 nm as protein denaturation occurred over a temperature range of 25 ℃ to 95 ℃. Each measurement is represented by the black, blue or red line. The first derivative was used to calculate the average $T_{1/2}$ for each construct. Figures are reprinted with permission from Lamantia, T.; Jansch, A.; Marsee, J. D.; Weiland, M. H.; Miller, J. M., Engineered Sphingomonas sp. KT-1 PahZ1 monomers efficiently degrade poly(aspartic acid). *Biophysical Chemistry* **2022,** *281*, 106745. Copyright 2022 Elsevier publishing.

3.3.4 Denaturation and Heat Precipitation Assay Analysis

Following the heat and chemical treatment assays, the stability of each construct was further assessed without regard to catalytic activity in a refolding experiment. Each protein was chemically denatured, and the chemical denaturant was then dialyzed out to assess overall protein recovery. The results, summarized in Table 2, show the average amount of protein that refolded. While similar overall, wild-type did have the highest recovery after denaturation. The IM had the most variability in recovery between trials, as seen by the large standard deviation, while E251K had the most consistency between trials.

Table 2. Quantification of protein recovered after denaturation with Gnd HCl.

	Wild-type	***E251K***	***IM***
Percent Recovered (%)	81.7 ± 1.8	80.5 ± 0.3	76.1 ± 7.6

The stability of each construct was then analyzed by looking at the amount of protein precipitated after heating compared to the amount of protein recovered after precipitation. As described in the methods, each construct was heated to precipitate the enzyme, centrifuged to pellet the enzyme, and then resuspended in 6 M Gnd-HCl before dialyzing. The results in Table 3 show that each construct did fully precipitate after heating. However, E251K had a significant increase in the amount of protein that was recovered compared to the IM or wild-type. The increased recovery of E251K as well as the GPC activity studies indicate that the amount of energy required for the monomer to properly refold is likely less than the energy needed for the dimer to refold, and further studies[21] found that there is a difference of 46 kJ/mol between the activation energies for the dimer and monomer. While this difference is a very small amount of energy, it affects the ability of the wild-type to properly refold and retain its catalytic activity as it requires more energy than the monomer.

Table 3. Quantification of protein precipitated and recovered after heat precipitation.

	Wild-type	***E251K***	***IM***
Percent Precipitated (%)	99.1 ± 0.1	98.7 ± 0.6	98.1 ± 0.1
Percent Recovered (%)	73.5 ± 9.3	89.5 ± 4.3	75.5 ± 5.5

3.4 Conclusion

While working to develop an enzyme capable of poly(aspartic acid) degradation in an industrial setting, destabilization of the dimeric state of $PahZ1_{KT\text{-}1}$ was a concern. Through protein engineering, the separation of the dimeric interface into monomeric units was possible, creating mutants E251K and IM.

The monomers exhibited catalytic activity similar to wild-type $PahZ1_{KT-1}$ when analyzed using GPC. When introduced to heat or chemical stress, a significant difference between the monomeric and dimeric state was shown, as the monomeric constructs retained activity while the wild-type had a loss of catalytic activity. While the amount of protein recovered after heat precipitation or chemical denaturation was not 100% for any of the constructs, E251K showed a significantly increased recovery (90%) compared to the other constructs after heat precipitation.

The creation of the $PahZ1_{KT-1}$ monomer is significant while working towards engineering enzymes capable of water-soluble degradation in a variety of conditions. The retention of catalytic activity and the ability of the enzyme to refold after introduction to stressors is desirable for many applications, and additional optimization could improve stability and catalytic activity further.

CHAPTER 4

CHARACTERIZATION OF PAHZ2$_{KT-1}$

4.1 PahZ2$_{KT-1}$ Introduction

PahZ2$_{KT-1}$ is the second poly(aspartic acid) hydrolase identified in the *Sphingomonas* bacteria strain. This enzyme acts upon oligo(aspartic acid) (OAA), which is tPAA that has been broken down by PahZ1$_{KT-1}$ first. In this study, OAA is also referred to as digested poly(aspartic acid), or dPAA. After initial crystallization conditions were identified by the Hauptman-Woodward Institute, the crystal structure was determined, and PahZ2$_{KT-1}$ is a dimer that is similar in structure to M28 metallopeptidases, meaning that metal ions are necessary in the catalytic domain for activity. This project focused on the characterization of PahZ2$_{KT-1}$ using activity assays to determine the ideal metal for activity and if catalytic activity could be enhanced in the presence of NaCl.

4.2 Methods

4.2.1 Transformation, Expression, and Purification of PahZ2$_{KT-1}$

Synthesis of each construct was performed by GenScript (Piscataway, NJ) using the pET15b vector with a 5' NdeI and 3' XhoI restriction site. The plasmid was transformed into BL21 (DE3) *E. coli* cells according to the NEB protocol (New England Biolabs, Ipswich, MA) with the following exceptions: 250 uL of SOC was added, no serial dilutions were performed, and 25 uL and 250 uL of transformed cells were spread onto 1.5% LB Agar selection plates with carbenicillin to incubate. A well isolated colony was selected to inoculate 50 mL of lysogeny broth (LB) media containing 50 µg/mL carbenicillin. The starter growth incubated overnight at 37 ℃, shaking at 225 rpm. Following overnight incubation, 12.5 mL of the starter growth was used to inoculate 500 mL of LB-carb in 2L expression flasks. Cells were grown at 37 ℃, 225 rpm until the optical density (O.D.$_{600}$) reached a range of 0.6 – 0.8. Once the ideal O.D.$_{600}$ was reached, each flask was induced with 0.1 mM isopropyl β-D-1-thiogalactopyranoside (IPTG, GoldBio, St. Louis, MO) and transferred to incubate at 20 ℃, 225 rpm for 4 hours. Cells were harvested through centrifugation at 10,000 xg for 20 min at 4 ℃, and then stored at -20 ℃.

The harvested cells were resuspended in start buffer (50 mM Tris, pH 8.0, 300 mM NaCl, and 20 mM imidazole), and lysed by sonication in an ice bath over a 45 min cycle with a 20 sec pulse, 59 sec rest, and 58% amplification. Following lysis, 125 units/mL of turbonuclease (Accelagen, San Diego, CA) and 10 µg/mL of lysozyme were added to enhance bacterial cell wall breakdown and remove genomic DNA. The cell lysate was rocked for 60 min at room temperature, then centrifuged at 10,000 xg for 20 min at 4 ℃ to pellet cell debris. The supernatant was loaded onto an AKTA FPLC with a HisPur Ni-nitriloacetic acid (NiNTA) column (Thermo Scientific, Waltham, MA) equilibrated in start buffer. The $PahZ1_{KT-1}$ protein was eluted from the NiNTA column using elution buffer (50 mM Tris, pH 8.0, 300 mM NaCl, 500 mM imidazole) over 60 min using a 0-100% gradient. Fractions of 3 mL were collected and run on a 12.5% SDS-PAGE at 150 V to analyze purity and identify elution peak on the corresponding purification chromatogram.

Following Ni-NTA purification, protein samples were initially dialyzed against 20 mM Tris, pH 7.4 to remove excess imidazole and then dialyzed against 50mM HEPES with 2 mM $ZnCl_2$, pH 7.0, to allow for PahZ2 constructs to bind the cofactor. Samples were then exhaustively dialyzed against 50mM HEPES, pH 7.0 and stored on ice prior to use in assays.

The DNA synthesis and site-directed mutagenesis of $PahZ2_{KT-1}$ constructs E155A, E156A, D121A, D122A_D184A, and E156A_H374A was also performed by GenScript. The transformation, expression, and purification protocol for each construct was the same as $PahZ2_{KT-1}$ wild-type.

4.2.2 GPC Activity Assays in the Presence of Metal

To determine if the metal present in the active site had an effect on catalytic activity, purified $PahZ2_{KT-1}$ was incubated overnight on ice in 50 mM HEPES pH 7.0 with different metals at a concentration of 50 mM, with the exception of Zn^{2+}. Due to the poor solubility of zinc, $PahZ2_{KT-1}$ was dialyzed against 50 mM HEPES, pH 7.0, 2 mM $ZnCl_2$, at 4 ℃. After the enzyme was incubated or dialyzed with a metal solution, 100 µL samples were set up with 24.5 mg dPAA and 80 µg of enzyme. Each sample incubated at 37 ℃ overnight, and then heated to 80 ℃ for 10 minutes to precipitate the enzyme and stop the reaction. Each sample was centrifuged at 17,000 xg for 1 min to pellet the

precipitated protein, and then stored at -80 ℃. Samples were spiked with 3 mg/mL thyroglobulin (MilliporeSigma, Burlington, MA), which served as the internal standard. Activity was analyzed by loading 10 µL of sample onto a Shimadzu GPC with a 3 µM SEC-2000, 300 mm x 7.8 mm column (Phenomonex, Torrance, A) equilibrated in 50 mM HEPES, pH 7.0. PahZ2$_{KT-1}$ forms aspartate as it degrades dPAA, and the amount formed was evaluated by analyzing the intensity of a peak at 11.18 minutes. The amount of product formed, percent activity, was calculated by comparing the ratio of the intensity of the internal standard at 5.0 minutes and the intensity of the peak at 11.18 minutes. The degradation of product was also analyzed as there was a decrease in dPAA oligomer peak height at 7.0 minutes. The percent of dPAA degraded was calculated by comparing a ratio of the peak intensity at 7.0 minutes and the intensity of the internal standard at 4.95 minutes. The greatest activity was seen in the presence of Zn^{2+} and all other samples were compared relative to the activity with Zn^{2+} bound.

4.2.3 GPC Activity Assays in the Presence of Salt

The substrate of PahZ2$_{KT-1}$, dPAA, must be digested by PahZ1$_{KT-1}$ first so that the enzyme can further break down the tPAA. To prepare the substrate, 0.05 mg/mL PahZ1$_{KT-1}$ was incubated with 100 mg/mL tPAA in 50 mM HEPES, pH 7.0, at 37 ℃ for 16 hours. PahZ1$_{KT-1}$ was heat precipitated at 90 ℃ for 15 minutes to stop the activity of the enzyme, and the dPAA substrate was centrifuged at 17,000 xg for 2 minutes to pellet the precipitated protein. The supernatant with the substrate was transferred to a new tube and lyophilized over 24 hours so that the dPAA could be stored and resuspended in buffer as needed.

The first assay was a timepoint assay to determine the PahZ2$_{KT-1}$ rate of degradation over a period of time with no salt present. PahZ2$_{KT-1}$ was prepared by dialyzing against 50 mM HEPES with 2 mM $ZnCl_2$ pH 7.0, then by exhaustively dialyzing against 50 mM HEPES, pH 7.0, to get rid of any unbound zinc ions. The lyophilized dPAA was resuspended to a final concentration of 100 mg/mL. Each assay sample was made by adding 24.5 mg of solubilized substrate and 0.1 mg/mL PahZ2$_{KT-1}$ with a final sample volume of 100 µL. Samples were incubated at 37 ℃ and 20 µL aliquots were taken at: 5 min, 30

min, 1 hr, 2 hrs, 3 hrs, 6 hrs, 12 hrs, and 24 hrs. The aliquots were heated to 90 ℃ for 10 minutes before centrifuging to pellet the denatured protein and storing at -80 ℃.

Before injecting 10 µL of sample onto the Shimadzu GPC with a Yarra 3 µM SEC-2000, 300 x 7.8 mm column (Phenomenex, Torrance, CA) equilibrated in 50 mM HEPES, pH 7.0, 10 µL of 4.4 mg/mL thyroglobulin internal standard was added to each sample. Each sample was detected by a refractive index detector, and analyzed by comparing the ratio of the internal standard and the product peak at a retention time of 11.02 min.

The next assay analyzed the activity of $PahZ2_{KT-1}$ in the presence of 150 mM NaCl and 500 mM NaCl to determine if salt had an effect on dPAA degradation in regards to rate or product formation. Samples were made following the same procedure as reported for the timepoint assay, but $PahZ2_{KT-1}$ was dialyzed against 50 mM HEPES pH 7.0 with 150 mM NaCl or 500 mM NaCl. The substrate was resuspended in the presence of salt, and each sample was made using the respective buffer to bring to a final sample volume of 100 µL. Analysis was performed in a similar manner, but due to a shift in the chromatogram with the presence of NaCl, the product peak for the 150 mM NaCl and 500 mM NaCl samples were analyzed at a retention time of 10.75 and 10.80 min, respectively.

4.2.4 GPC Activity Assays with $PahZ2_{KT-1}$ Catalytic Mutants

To confirm that residues identified through molecular dynamic studies played a significant role in the catalytic activity of the enzyme, an activity assay was performed with the following mutated constructs: E155A, E156A, D121A, D122A_D184A, and E156A_H374A. Samples were made following the same procedure as the timepoint assay for $PahZ2_{KT-1}$ wild-type (Section 4.2.3), however each catalytic mutant was incubated at 37 ℃ for only 24 hrs with 24.5 mg dPAA in 50 mM HEPES pH 7.0 with 0 mM NaCl. Samples were analyzed using the ratio of the internal standard and a retention time of 7.0 min due to a lack of product peak formation.

4.2.5 Dynamic Light Scattering Experiments

To determine if differing concentrations of NaCl would disrupt the dimeric structure of $PahZ2_{KT-1}$, a variety of samples were analyzed using Dynamic Light Scattering (DLS). Purified $PahZ2_{KT-1}$ at a

concentration of 2 mg/mL was dialyzed in 50 mM HEPES, pH 7.0, or in 50 mM HEPES 2mM $ZnCl_2$, pH 7.0 overnight at 4 ℃. Protein was removed from dialysis and precipitant was pelleted using centrifugation at 17,000 xg for 5 min at room temperature. Samples were set up as 1.0 mL samples with varying concentrations of NaCl. The first three samples contained $PahZ2_{KT-1}$ dialyzed without $ZnCl_2$ with 0 mM NaCl, 150 mM NaCl, or 500 mM NaCl, pH 7.0. The next three samples contained $PahZ2_{KT-1}$ dialyzed with $ZnCl_2$ 0 mM NaCl, 150 mM NaCl, or 500 mM NaCl, pH 7.0. Samples were made by first adding the enzyme, substrate, and then buffer. As the buffer was added, the samples were vortexed at a speed of 3 and the buffer was added in drop by drop. All samples were incubated on ice for 30 minutes, then precipitant was removed by centrifugation at 17g for 5 min at room temperature. More precipitant was observed in the samples containing 150 mM NaCl with $ZnCl_2$ and 500 mM NaCl with $ZnCl_2$ when compared to all other samples. Samples were placed on ice overnight before running on the dynamic light scattering (DLS) instrument.

4.3 Results and Discussion

4.3.1 $PahZ2_{KT-1}$ Crystal Structure

Crystal structure leads were initially identified by the Hauptman-Woodward Institute High-Throughout Crystallization Screening Center where a variety of conditions were tested. There were a variety of conditions identified that produced single crystals.

Dr. Wallen, a collaborator at Western Carolina University, determined the crystal structure of $PahZ2_{KT-1}$ to 1.85 Å. The initial structure showed one Gd^{3+} or Sm^{3+} bound in the catalytic site, with diffraction to 1.85 Å, while the second structure had two Zn^{2+} bound and diffracted to 2.5 Å. The $PahZ2_{KT-1}$ crystal structure, shown in Figure 13, is made up of two monomers that are joined at a dimeric face that have 2-fold rotational symmetry. The monomeric units each contain a dimerization domain and a catalytic domain, which are connected by a hinge region in the middle. The catalytic domain, which has a positively charged surface, was identified as residues M1-G195, and G319-Q405. Two zinc atoms associate with each monomer unit and are necessary for degradation of dPAA. The presence of the bound

metal for degradation to occur is consistent with a metalloprotease, and was further analyzed through analysis using GPC with different metals present.

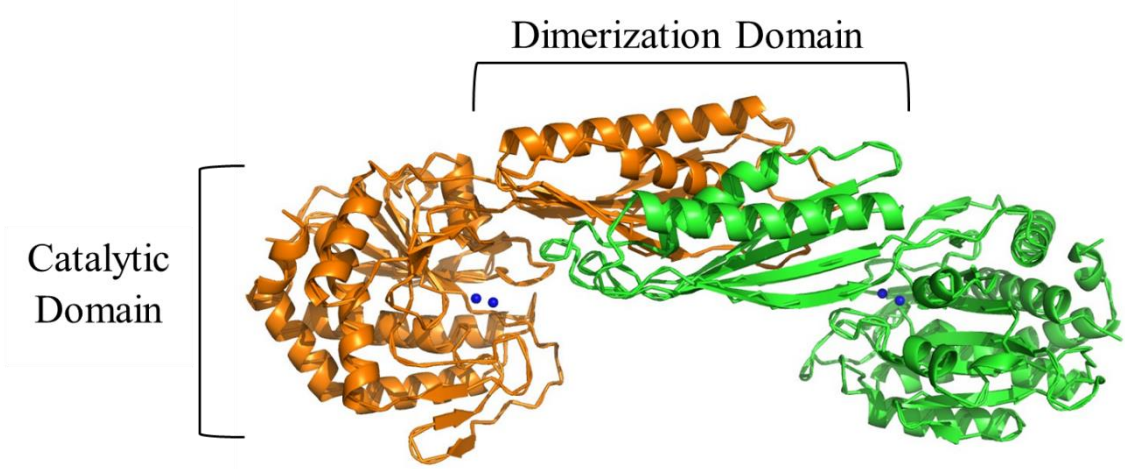

Figure 13. Cartoon representation of the PahZ2$_{KT-1}$ crystal structure. The structure is a dimer, with each monomer shown in orange and green. Bound zinc in the catalytic active sites are shown as blue spheres. The dimerization domains and catalytic domains are highlighted by the brackets.

4.3.2 PahZ2$_{KT-1}$ Catalytic Site Analysis

As an M28 metallopeptidase, PahZ2$_{KT-1}$ is expected to bind a metal for catalytic activity. In initial crystal structures, Gd^{3+} or Sm^{3+} was bound at the active site with coordinating residues highlighted in Figure 14A. Due to the similar size of Gd^{3+}/Sm^{3+}, it was not clear which metal was bound, but there was only one metal ion present in the active site. The Gd^{3+} /Sm^{3+} was then displaced, and replaced with two zinc ions, Figure 14B. With zinc ions present, each coordinates in a tetrahedral molecular geometry, which was predicted to be a preferred coordination that is commonly seen with M28 metallopeptidases. An overlay with Gd^{3+}/Sm^{3+} and Zn^{2+} is shown in Figure 14C to show differences in the placement of the metals, while there is no difference in side-chain positioning. With the Gd^{3+}/Sm^{3+} complex, there are seven interactions with side chain residues E155, D184, H94, D121, and E156, as well as interactions with two water molecules. The zinc-bound complex shows two zinc ions, in which the Zn_I coordination site interacts with side chain residues H94, D184 and D121, and the Zn_{II} coordination site interacts with side chain residues H374, E156, and D121.

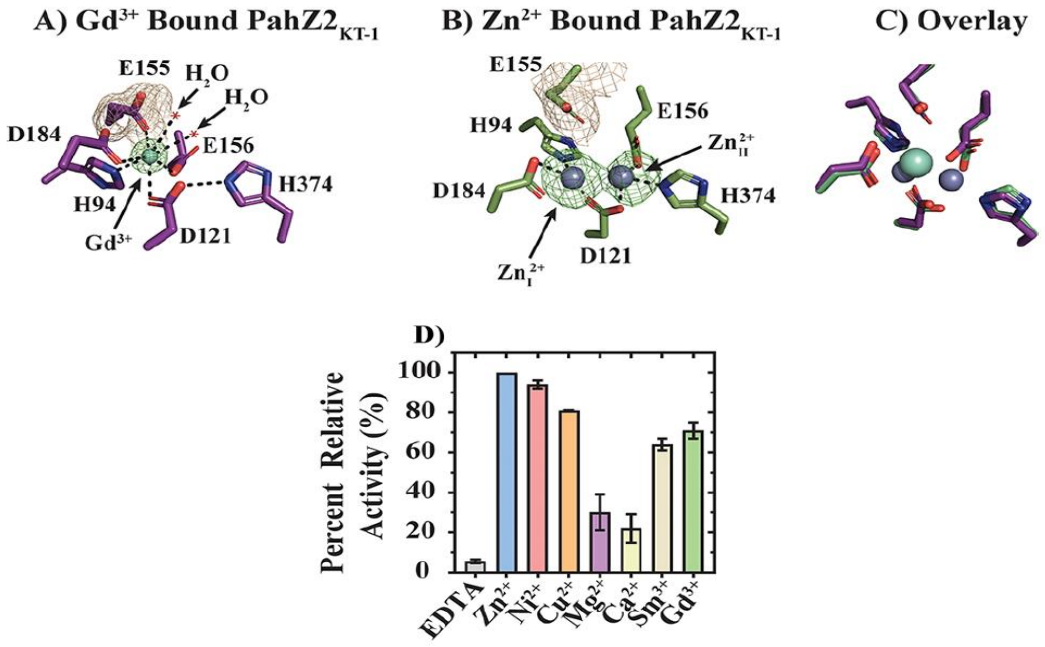

Figure 14. PahZ2$_{KT-1}$ catalytic active site analysis. A) Stick model representation of the active site with Gd^{3+}/Sm^{3+} bound. B) Stick model representation of the active site with Zn^{2+} bound. C) Overlay of the active site and corresponding residues with Gd^{3+}/Sm^{3+} compared to Zn^{2+} bound. D) Degradation of dPAA represented as percent relative activity with different metals bound in the PahZ2$_{KT-1}$ catalytic site. Error bars represent the standard deviation between triplicate measurements. Figures are reprinted with permission from Brambley, C. A.; Yared, T. J.; Gonzalez, M.; Jansch, A. L.; Wallen, J. R.; Weiland, M. H.; Miller, J. M., Sphingomonas sp. KT-1 PahZ2 Structure Reveals a Role for Conformational Dynamics in Peptide Bond Hydrolysis. *J Phys Chem B* **2021,** *125* (22), 5722-5739. Copyright 2021 American Chemical Society.

Due to the tetrahedral arrangement of the zinc atoms in each monomeric unit, there may be other metals that could interact with PahZ2$_{KT-1}$ and retain the overall function of the enzyme. In previous reports[22], an M28 metalloprotein homologous to PahZ2$_{KT-1}$ retained activity in the presence of Co^{2+}, Zn^{2+}, Cd^{2+}, Mn^{2+}, Ni^{2+}, and Mg^{2+} metal ions. With this information, an activity assay was performed in the presence of similar metal ions to see if PahZ2$_{KT-1}$ retained activity, results shown in Figure 14D. The enzyme was dialyzed against 50 mM HEPES pH 7.0 with excess amounts of ethlyenediamine tetraacetic acid (EDTA), Cu^{2+}, Ni^{2+}, Mg^{2+}, Ca^{2+}, Zn^{2+}, Sm^{3+}, or Gd^{3+}. EDTA was used to determine if activity was truly dependent on the presence of a metal ion, as it chelated any metals present and was shown to significantly inhibit degradation of the substrate. The loss of activity in the presence of EDTA supports the M28 family member classification of PahZ2$_{KT-1}$, and that metal ions are necessary for catalytic

activity. Different coordination geometries occurred with different metals, and therefore altered the relative activity when geometries other than tetrahedral were adopted. Metals that were likely to form a tetrahedral coordination geometry had significantly more catalytic activity than those that did not. $Sm^{3+}$and Gd^{3+} do not form tetrahedral complexes and instead form complexes with coordination geometries ranging from 6 to 8. The Sm^{3+}or Gd^{3+} bind directly to the Z_I site, and then interact with residue E156 in the Zn_{II} site, blocking any other metal from binding, and therefore retaining activity only associated with a single bound metal ion on each monomeric unit.

4.3.3 PahZ2$_{KT-1}$ Catalytic Site Mutagenesis

To confirm the importance of the identified residues interacting with the zinc binding sites, the following mutations were introduced: E155A, E156A, D121A, D122AD184A, and E156AH374A. Each residue was mutated to an alanine to disrupt any side chain interaction at that specific residue. The constructs with two mutations were designed to disrupt the ability for zinc to bind at the Zn_I or Zn_{II} site. Each construct was incubated with dPAA for 24 hours and analyzed using GPC analysis. The data, Figure 15, shows that each mutated construct had a significant decrease in activity compared to wild-type PahZ2$_{KT-1}$. Construct D121A had the most activity at 6.5 ± 0.5%, while the percent relative activity for E155A and E156A was 0.6 ± 0.2% and 1.1 ± 0.3%, respectively. The double mutations had a similar decrease in overall activity, with D122A_D184A at 5.9 ± 0.3% and E156A_H372A at 1.3 ± 0.6%. While there is significant loss of activity with each mutation, the mutations at the Zn_{II} site have a greater decrease in activity compared to the activity

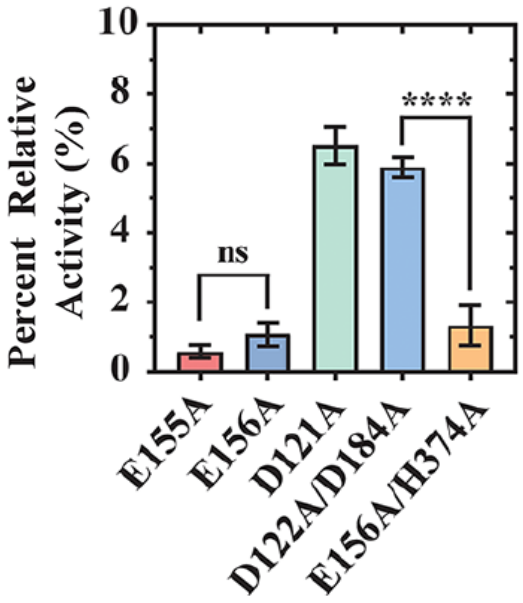

Figure 15. GPC activity analysis of catalytic mutants compared to wild-type PahZ2$_{KT-1}$. The relative activity is significantly decreased when identified residues are mutated. Error bars represent the standard deviation between triplicate measurements. Figures are reprinted with permission from Brambley, C. A.; Yared, T. J.; Gonzalez, M.; Jansch, A. L.; Wallen, J. R.; Weiland, M. H.; Miller, J. M., Sphingomonas sp. KT-1 PahZ2 Structure Reveals a Role for Conformational Dynamics in Peptide Bond Hydrolysis. *J Phys Chem B* **2021,** *125* (22), 5722-5739. Copyright 2021 American Chemical Society.

when mutations are introduced to the Zn_I site. The overall significant loss of activity with the introduced mutations confirm that the residues are part of the catalytic active site.

4.3.4 NaCl Enhances PahZ2$_{KT-1}$ Rate of Degradation

The degradation of dPAA was analyzed with and without the presence of NaCl. PahZ2$_{KT-1}$ would likely be introduced to salt ions when functioning under physiological conditions, and there had been no previous studies related to enzyme activity in the presence of salt. To determine if the presence of NaCl does in fact have an impact on activity, GPC activtiy assays were performed with enzyme that was incubated in varying salt concentrations: 0 mM NaCl, 150 mM NaCl, and 500 mM NaCl. For each salt concentration, timepoints were collected to determine if there was a change in the amount of dPAA degraded or the rate of degradation. The intensity of the aspartic acid peak, Figure 16, was used to analyze the amount of product formed, which took place at a timepoint of 11.18 minutes with 0 mM NaCl and 10.80 minutes with 150 mM and 500 mM NaCl. The slight shift in retention time was due to the presence of NaCl as well as a change in columns between samples run on the GPC with no salt present and with salt present. There was a very low yield of aspartic acid formed, therefore analysis was also performed by looking at loss of dPAA, or total degradation compared to the control with no enzyme present.

Analysis of product formation was plotted in Figure 17, which illustrates the relative activity of PahZ2$_{KT-1}$ in each NaCl condition, along with the differences in rate as of degradation as the concentration of NaCl increased. The slope of the line was determined from an incubation time of 360 minutes to 1500 minutes, and was used to estimate the reaction intitial velocity, Figure 17D. There is a linear and positive increase in initial velocity seen as the concentration of NaCl increases, which suggests that the presence of NaCl enhances the activity of PahZ2$_{KT-1}$ without inhibiting the formation of product.

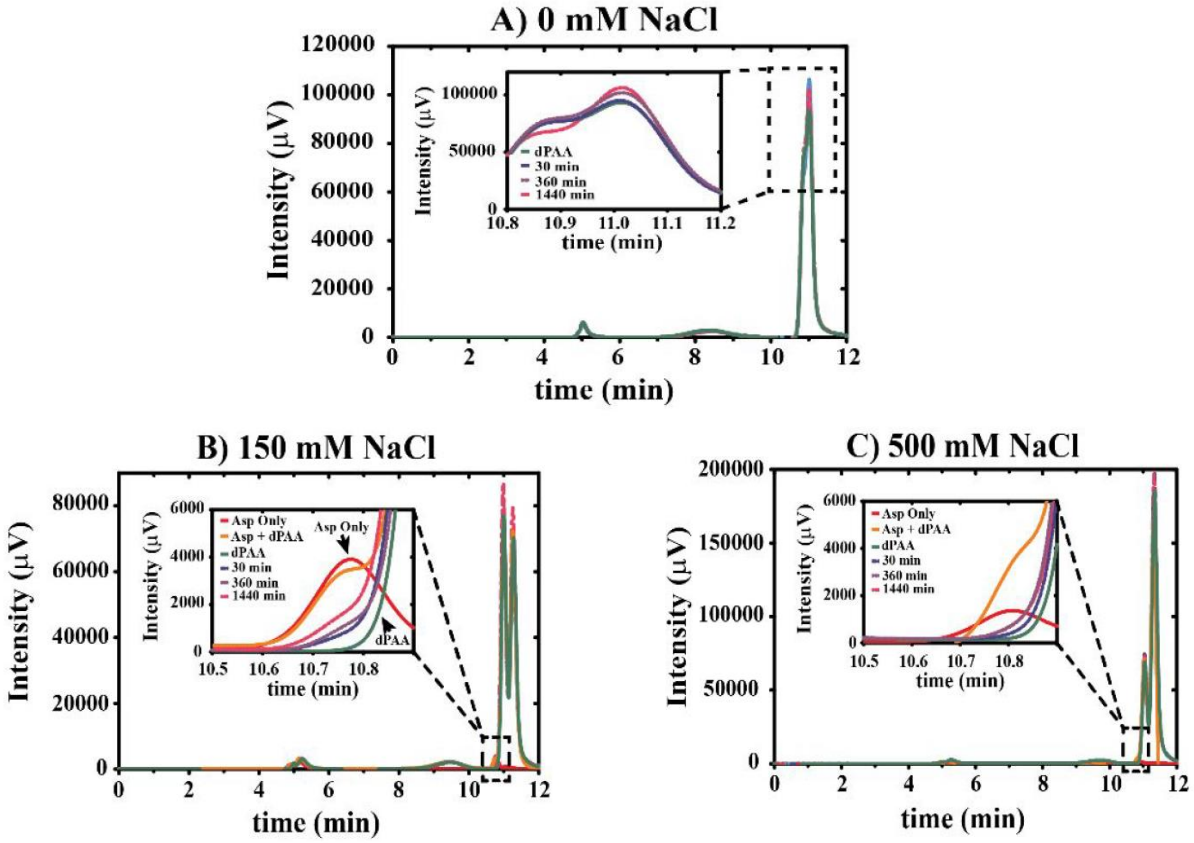

Figure 16. Representative chromatograms of $PahZ2_{KT-1}$ aspartic acid formation. A) Product formation in the absence of NaCl. Increased product is shown as incubation time of dPAA with $PahZ2_{KT-1}$ is increased. B) Product formation in the presence of 150 mM NaCl. Aspartic acid with no enzyme or dPAA present is shown in red at an elution time of 10.75 minutes, and aspartic acid with dPAA and no enzyme is shown in yellow. The aspartic acid was run by itself to be used as a reference of where the product was eluting. An increase in product formation can be seen as enzyme incubation time increases. C) Product formation in the presence of 500 mM NaCl. The monomeric aspartic acid is slightly shifted to the right, with an elution time of 10.8 minutes. Analysis of activity took place at the elution time of monomeric aspartic acid control. Figures are reprinted with permission from Brambley, C. A.; Yared, T. J.; Gonzalez, M.; Jansch, A. L.; Wallen, J. R.; Weiland, M. H.; Miller, J. M., Sphingomonas sp. KT-1 PahZ2 Structure Reveals a Role for Conformational Dynamics in Peptide Bond Hydrolysis. *J Phys Chem B* **2021,** *125* (22), 5722-5739. Copyright 2021 American Chemical Society.

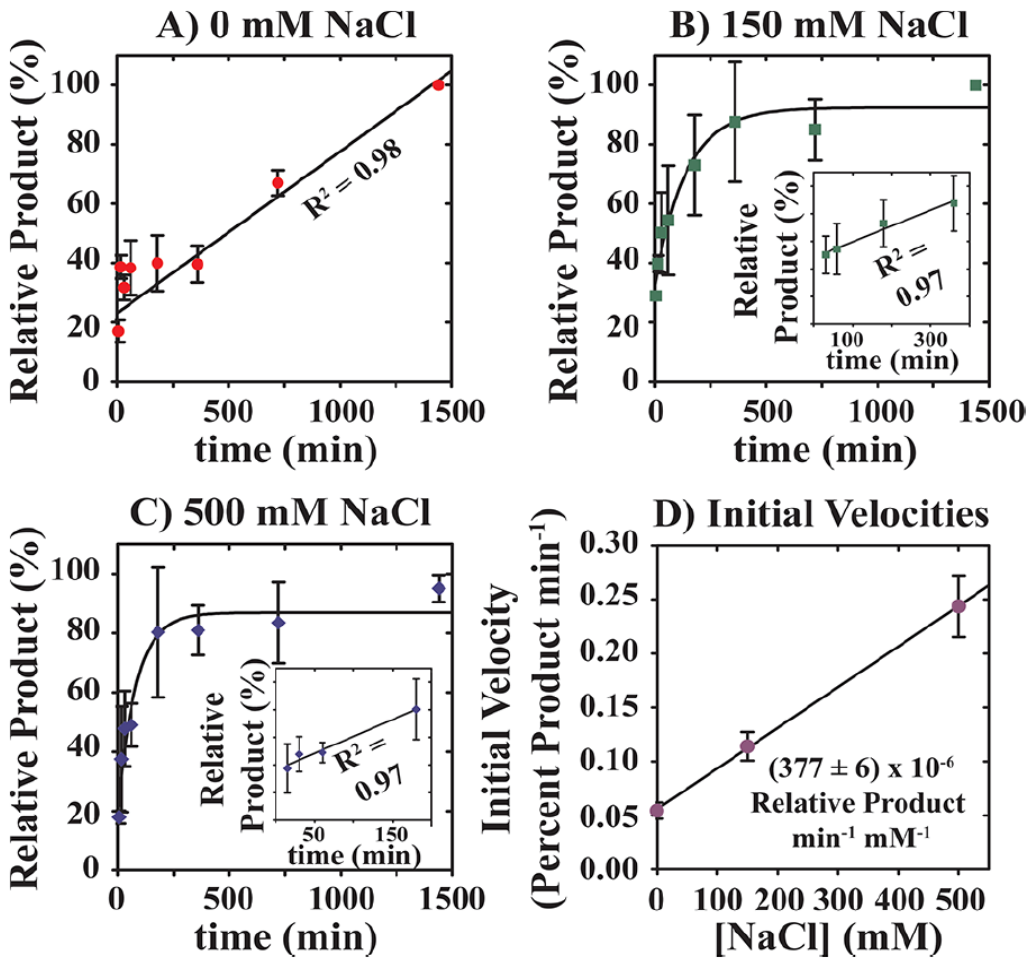

Figure 17. GPC analysis of dPAA degradation in various NaCl concentrations. A-C) Percent relative product formed at specific incubation times in the presence of 0 mM NaCl (A), 150 mM NaCl (B), and 500 mM NaCl (C). The error bars on each plot represent the standard deviation from triplicate measurements. D) Calculation of intitial velocity represented as a plot to show the difference between concentration of NaCl (mM) and amount of relative product formed per minute (min^{-1} mM^{-1}). Figures are reprinted with permission from Brambley, C. A.; Yared, T. J.; Gonzalez, M.; Jansch, A. L.; Wallen, J. R.; Weiland, M. H.; Miller, J. M., Sphingomonas sp. KT-1 PahZ2 Structure Reveals a Role for Conformational Dynamics in Peptide Bond Hydrolysis. *J Phys Chem B* **2021,** *125* (22), 5722-5739. Copyright 2021 American Chemical Society.

4.3.5 PahZ2$_{KT-1}$ Conformation Changes in the Presence of NaCl

The enhanced rate of degradation in the presence of NaCl was determined to occur due to a conformation change. Molecular dynamic studies were performed by a collaborator, Dr. Miller at Middle Tennessee State University, to model the conformational changes that occur when NaCl is present. In the absence of salt, PahZ2$_{KT-1}$ adapts an open conformation when dPAA is bound. The interaction between

the dPAA substrate, catalytic active site, and substrate binding residues is modeled in Figure 18A when no salt is present. In the open conformation, hydrogen bonding occurs between the dPAA and residues R270, R316, S356, R162, and R165. While R270 and R316 are part of the dimerization domain, S356 is a residue present in the hinge region of the enzyme. R162 and R165 make up residues present on the catalytic domain.

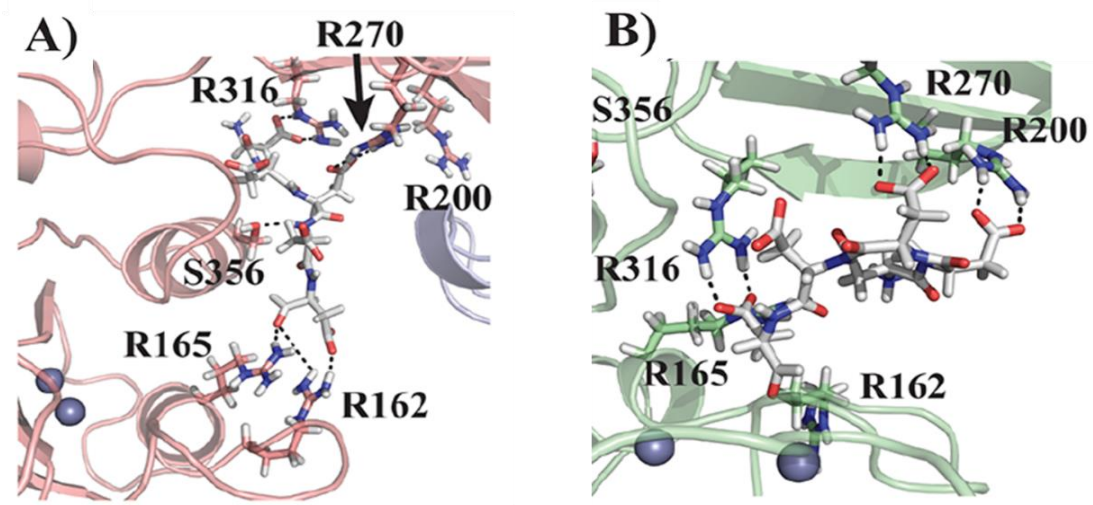

Figure 18. Stick model highlighting PahZ2$_{KT-1}$ conformational change in the absence and presence of NaCl. A) dPAA position in the absence of NaCl. Hydrogen bonding between the enzyme and dPAA substrate is occuring at residues R162, R165, S356, R270, and R316. The zinc ions bound to the active site are represented by spheres (slate). B) dPAA position in the presence of NaCl. A conformational change can be seen by the change in hydrogen bonding that is occuring between the enzyme and dPAA, as well as by the closer location of the zinc ions (slate spheres) in the catalytic active site. Hydrogen bonding is now occuring between dPAA and residues R162, R165, R316, R200 and R270, and there is no longer interaction with S356 along the hinge region of the enzyme. Figures are reprinted with permission from Brambley, C. A.; Yared, T. J.; Gonzalez, M.; Jansch, A. L.; Wallen, J. R.; Weiland, M. H.; Miller, J. M., Sphingomonas sp. KT-1 PahZ2 Structure Reveals a Role for Conformational Dynamics in Peptide Bond Hydrolysis. *J Phys Chem B* **2021,** *125* (22), 5722-5739. Copyright 2021 American Chemical Society.

When NaCl is present, the enzyme conformation changes to a closed conformation. In the closed conformation, the catalytic domain moves closer in proximity to the dimerization domain, closing at the hinge region. This conformation changes brings the dPAA substrate closer to the zinc bound active site, and eliminates interactions occuring between the substrate and the hinge region of the enzyme. Figure 18B illustrates this conformational change, with interactions occuring at dimerization domain residues

R270, R200, and R316, along with interactions at the catalytic domain with residues R162 and R165. The closed conformation seems to directly affect catalytic acitivty, as seen by the increased rates of degradation reported in the previous section.

4.3.6 DLS Studies Confirm Dimeric Structure is not Disrupted in the Presence of Salt

The presence of salt can disrupt dimer formation by interferring with electrostatic interactions. To confirm that the dimeric structure was not disrupted in the presence of NaCl, DLS experiments were performed to compare particle diameter in various salt concentrations. Figure 19 shows the DLS study results by plotting the signal intensity compared to particle diameter. With 0 mM NaCl, the particle diameter mean is 8.8 ± 0.7 nm. In the presence of 150 mM NaCl and 500 mM NaCl, the mean particle diameters are 8.9 ± 0.9 nm and 10.0 ± 2.0 nm, respectively. Statistical testing performed indicates that there is no significant difference in PahZ2$_{KT-1}$ particle diameter in the absence or presence of NaCl.

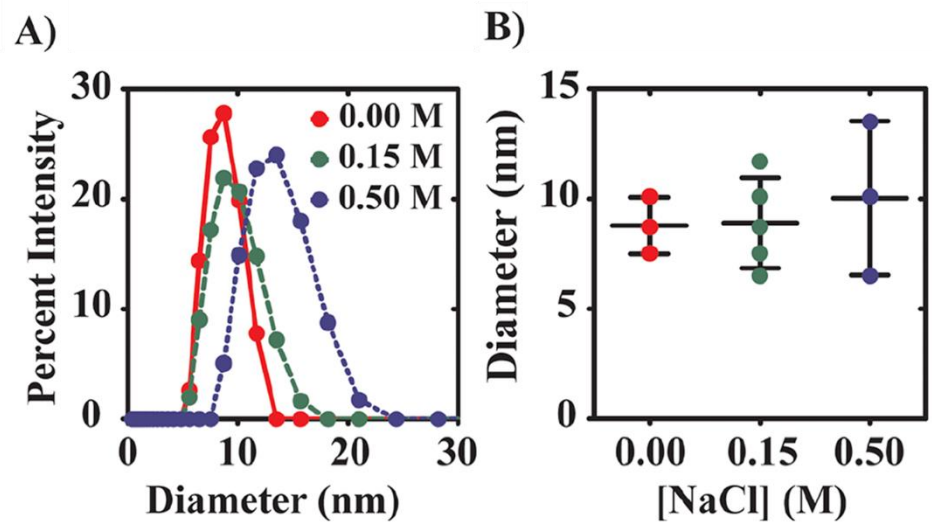

Figure 19. Impact on the dimeric structure of PahZ2$_{KT-1}$ with the addition of NaCl. A) Plot showing the results of Dynamic Light Scattering (DLS) experiments with varying concentrations of NaCl. B) Plot of particle size measurements (single sphere) as the presence of NaCl increased. The horizontal lines represent mean and standard deviation of each triplicate measurement. Dimer integrity is not disrupted by the presence of salt, and there is no significant difference between particle diameters. Figures are reprinted with permission from Brambley, C. A.; Yared, T. J.; Gonzalez, M.; Jansch, A. L.; Wallen, J. R.; Weiland, M. H.; Miller, J. M., Sphingomonas sp. KT-1 PahZ2 Structure Reveals a Role for Conformational Dynamics in Peptide Bond Hydrolysis. *J Phys Chem B* **2021,** *125* (22), 5722-5739. Copyright 2021 American Chemical Society.

4.4 Conclusion

$PahZ2_{KT-1}$, an enzyme that acts upon PAA first digested by $PahZ1_{KT-1}$, is characterized as an M28 metallopeptidase. The X-ray crystal structure reveals that the enzyme is a dimer, made up of a dimerization domain and a catalytic domain with two-fold rotational symmetry. Optimal activity occurs when there are two zinc ions bound at the catalytic active site, which is consistent with an M28 classification. The presence of NaCl enhances the activity of $PahZ2_{KT-1}$, as the enzyme adopts a closed conformation, bringing the catalytic active site closer to the substrate binding residues present along the dimerization domain. The increased rate of degradation as the concentration of NaCl increases suggests stabilization of the enzyme when in a closed state. With the knowledge of the crystal structure and conformational changes, further research can occur to enhance the formation of free aspartic acid. Characterization of $PahZ2_{KT-1}$ provides knowledge that can be built upon to improve the enzyme and continue to move towards the goal of water-soluble polymer degradation.

CHAPTER 5

ANALYSIS OF PAHZ2$_{KT-1}$ SUBSTRATE BINDING

5.1 Introduction

5.1.1 Mutating the PahZ2$_{KT-1}$ Substrate Binding Site

The structure of PahZ2$_{KT-1}$ was solved in the previous study and found to be a member of the M28 metalloprotease family, meaning two Zn^{2+} must be present in the active site for catalytic activity. The presence of sodium chloride enhanced catalytic activity by promoting the formation of a closed enzyme complex. In molecular docking studies, from which the substrate binding site residues were predicted, the polyanionic PAA substrate positioned itself along a trough of arginine residues that directed the PAA toward the catalytic active site.[23] With the predicted residues identified, the purpose of this study is to confirm the residues important to substrate binding with the intention of engineering a more efficient enzyme.

5.2 Methods

5.2.1 Transformation, Expression, and Purification of PahZ2$_{KT-1}$

Synthesis of each construct was performed by GenScript (Piscataway, NJ) using the pET15b vector with a 5' NdeI and 3' XhoI restriction site. The transformation, expression, and purification protocol was the same as previously mentioned with wild-type PahZ2$_{KT-1}$ (Chapter 4, section 4.2.1).

5.2.2 GPC Activity Assays in the presence of Salt

The substrate, dPAA, was prepared in the same manner as with the wild-type (Chapter 4, section 4.2.2), 0.05 mg/mL PahZ1$_{KT-1}$ was incubated with 100 mg/mL tPAA in 50 mM HEPES, pH 7.0, at 37 ℃ for 16 hours. PahZ1$_{KT-1}$ was heat precipitated at 90 ℃ for 15 minutes, and the dPAA substrate was centrifuged at 17,000 xg for 2 minutes to pellet the precipitated protein. The supernatant with the substrate was transferred to a new tube and lyophilized over 24 hours so that the dPAA could be stored and resuspended in buffer as needed.

The first assay was performed to determine the amount of dPAA degraded by each construct with no salt present. Each construct, along with the wild-type, was prepared by dialyzing against 50 mM HEPES with 2 mM $ZnCl_2$ pH 7.0, then exhaustively dialyzing against 50 mM HEPES pH 7.0. The previously lyophilized dPAA was resuspended to a final concentration of 100 mg/mL. Each assay sample was made by adding 24.5 mg of solubilized substrate and 0.1 mg/mL enzyme with a final volume of 100 µL. Samples were incubated at 37 ℃ and removed at 24, 48, and 96 hr. The samples were heated to 90 ℃ for 10 minutes and then centrifuged to pellet the denatured protein. Samples were stored at -80 ℃ until run on the GPC.

Before injecting 10 µL of sample onto the Shimadzu GPC with a Yarra 3 µM SEC-2000, 300 x 7.8 mm column (Phenomenex, Torrance, CA) equilibrated in 50 mM HEPES pH 7.0, 10 µL of 4.4 mg/mL thyroglobulin internal standard was added to each sample. Each sample was detected by a refractive index detector and analyzed by comparing the ratio of the area under the internal standard peak from a retention time of 4.5 min to 6.0 min, and the area under the dPAA peak from a retention time of 6.0 min to 9.8 min. Constructs that showed significant degradation were further analyzed in a timepoint assay.

The next assay analyzed the activity of each construct in the presence of 150 mM NaCl and 500 mM NaCl to determine if salt had an effect on dPAA degradation in regards to rate or product formation. Samples were made following the same procedure as reported for the assay with no salt, but each enzyme was dialyzed against 50 mM HEPES pH 7.0 with 150 mM NaCl or 500 mM NaCl. The substrate was resuspended in the presence of salt, and each sample was made using the respective buffer to bring to a final volume of 100 µL. Analysis was performed in a similar manner by comparing the degradation of dPAA to the wild-type.

5.2.3 Further GPC Analysis of Constructs with Significant Activity

Constructs that showed significant activity at an enzyme concentration of 0.1 mg/mL were further analyzed in a timepoint assay. Each construct, along with the wild-type, was prepared by dialyzing against 50 mM HEPES with 2 mM $ZnCl_2$ pH 7.0, then by exhaustively dialyzing against 50 mM HEPES

pH 7.0. The previously lyophilized dPAA was resuspended to a final concentration of 100 mg/mL. Each assay sample was then made by adding 24.5 mg of solubilized substrate and 0.01 mg/mL enzyme with a final sample volume of 100 µL. Samples were incubated at 37 ℃ and taken out at the following timepoints: 15 min, 30 min, 1 hr, 3 hr, 4 hr, 6 hr, 12 hr, 24 hr, 48 hr, and 96 hr. Each sample was heated to 90 ℃ for 10 minutes and then centrifuged to pellet the denatured protein. Samples were stored at -80 ℃ until run on the GPC.

An assay was performed in the presence of 150 mM NaCl, as well as 500 mM NaCl using the same methods and timepoints. Analysis compared the area of the internal standard to the area of the dPAA peak, at the same retention times as reported in the previous section (Chapter 5, section 5.2.2).

5.3 Results and Discussion

5.3.1 Mutations to the Substrate Binding Site Dictate Activity

In previous studies[23], the presence of NaCl was shown to enhance catalytic activity of wild-type PahZ2$_{KT-1}$ due to stabilization of the hinge region between the dimerization domain and catalytic domain. Substrate binding site residues were predicted based on molecular modeling studies, and further analyzed through GPC studies to determine if the introduction of point mutations could lead to the engineering of a more efficient enzyme. During GPC analysis, dPAA degradation was studied for each mutated construct in the presence of 0 mM NaCl, 150 mM NaCl, and 500 mM NaCl by comparing the dPAA peak area as time increased, representative chromatogram shown in Figure 20. Mutants R200A,

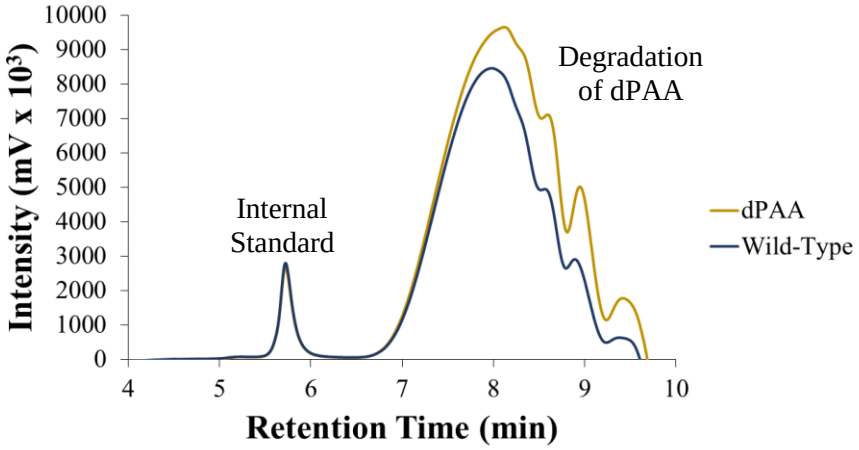

Figure 20. Representative chromatogram of PahZ2$_{KT-1}$ dPAA degradation. The area under the dPAA peak was used for analysis of relative activity, dPAA with no enzyme is shown in gold, and dPAA after incubation with PahZ2$_{KT-1}$ is shown in blue. The internal standard shown at 5.7 minutes, thyroglobulin, was used to correct for chromatographic shifts or differences in load amount.

R200E, R270A, R270E, R316A, R316E, R200AR270AR316A, and R200ER270ER316E all showed a significant decrease in activity, as shown in Figure 21. Most of the constructs did show enhanced activity in the presence of salt, but still less than 60% total dPAA degradation compared to the wild-type. Constructs that showed similar activity, greater than 70% degradation at 24 hrs, to wild-type were further analyzed in a timepoint assay.

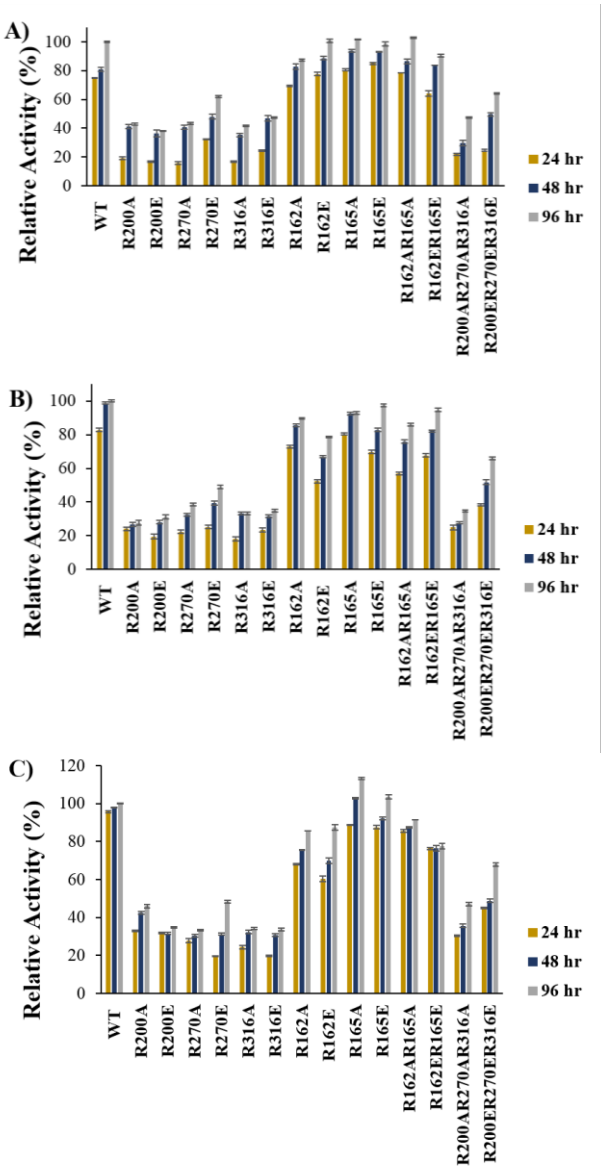

Figure 21. Results of the GPC activity assay showing relative activity of each mutated construct. A.) Degradation in the presence of 0 mM NaCl at a concentration of 0.1 mg/mL. B.) Degradation in the presence of 150 mM NaCl. C.) Degradation in the presence of 500 mM NaCl.

Loss in relative activity confirms the roll of each residue in regards to substrate binding. While not part of the catalytic active site, each positively charged arginine residue was predicted to direct the polyanionic substrate to the active site. When mutated to an alanine or glutamic acid, activity loss was predicted as the polyanionic substrate would no longer be attracted to the residue, and in the case of glutamic acid it would be repelled. Residues R165A, R162A, R165E, R162E, R162AR165A, and R162ER165E seem to play less of role in directing the substrate, as each construct had similar activity compared to the wild-type.

5.3.2 Construct R165A Shows Increased Rate Compared to Wild-type

Constructs R162A, R165A, R162E, R165E, R162AR165A, and R162ER165E were analyzed in a timepoint assay at a concentration of 0.01 mg/mL over a 96 hr time period, and R165A was the only

construct with an increased rate of degradation in the presence of salt. As shown in Figure 22, R165A had no significant loss of activity at a lower concentration like the other constructs when salt was added. Activity was similar to that shown in the previous assay without the presence of salt, but R162A and R162AR165A had a significant decrease in activity when introduced to salt at a lower concentration. The loss of activity with R162A, R162E, R162AR165A, and R162ER165E may have been due to the low enzyme concentration. At a lower concentration, the salt is likely inhibiting enzyme activity through electrostatic interactions. The loss of activity was not observed at the higher enzyme concentration of 0.1 mg/mL, and further timepoint studies at a higher concentration are necessary to further characterize the loss of activity.

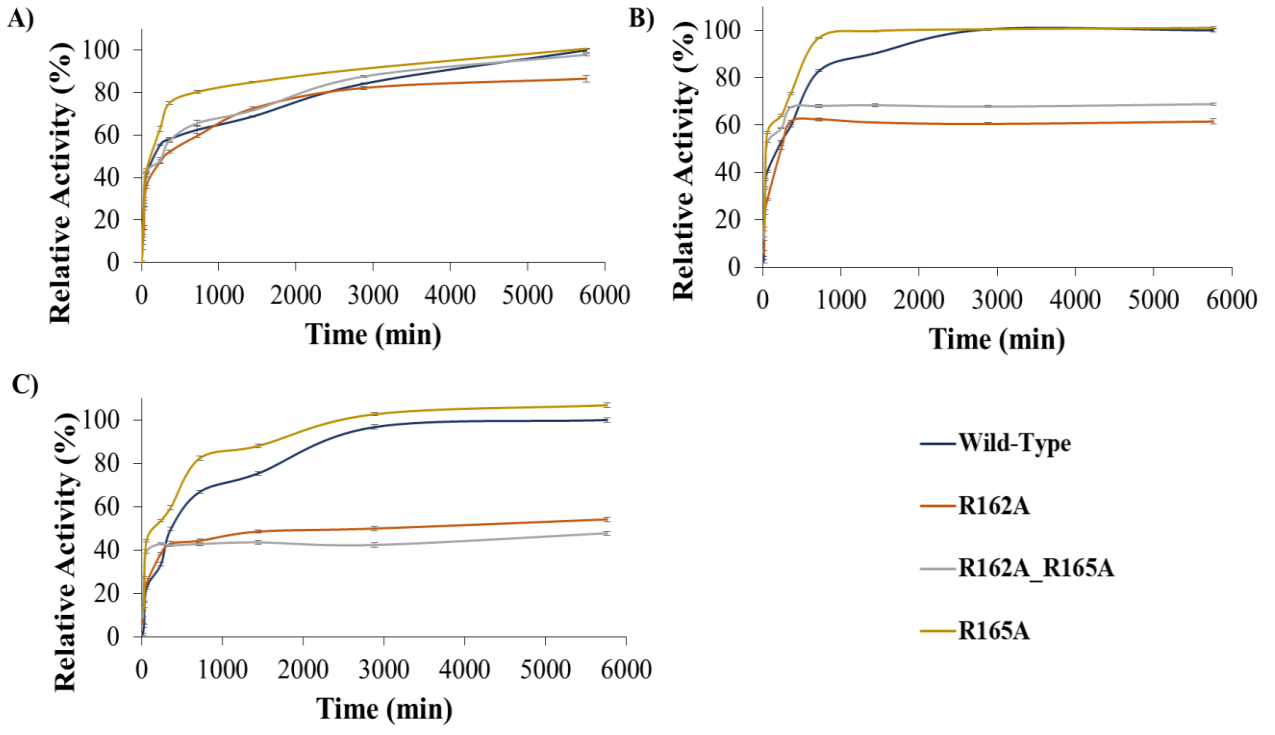

Figure 22. GPC activity analysis of PahZ2$_{KT-1}$ constructs with activity similar to wild-type. A.) Construct degradation without NaCl present. Rate enhancement is seen with R165A, which reaches a terminal point prior to wild-type. B.) Degradation in the presence of 150 mM NaCl, with R165A still showing enhanced rate. R162A and R162AR165A show a significant loss of activity with the addition of salt. C.) dPAA degradation in the presence of 500 mM NaCl. R165A shows increased rate, while activity of R162A and R162AR165A drops below 50% compared to wild-type.

The rate enhancement of R165A is likely due to a decreased interaction with the substrate. The positively charged arginine present in the wild-type is holding on to the negatively charged substrate, and not releasing the substrate after it has been cleaved. With the R165 residue becoming neutral, and much shorter in length, the substrate is easily released by the enzyme after cleavage, allowing for another chain to occupy the substrate binding site for degradation.

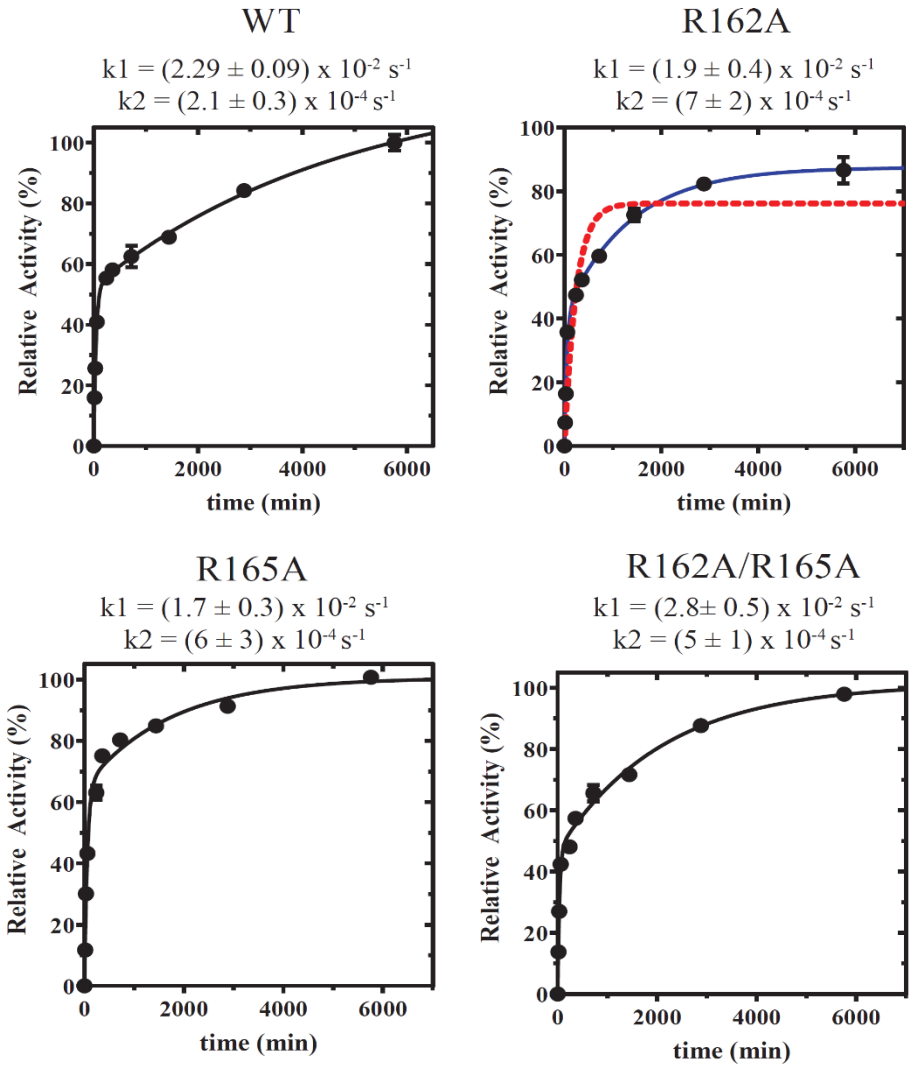

Figure 23. PahZ2$_{KT-1}$ rate analysis using a double-exponential model. Each construct rate was analyzed and can be divided into two different phases. The first phase, prior to 24 hours, is described as the fast phase, or k1. The second phase, 24 hours to 96 hours, is described as the slow phase, or k2. The red dotted line included with R162A is an example of what a single-exponential rate model looks like applied to the data.

With no salt present, each construct reached an endpoint similar to $PahZ2_{KT-1}$ wild-type. A rate analysis was performed on each construct using the relative activity compared to time from Figure 22A. The results of the rate analysis are shown in Figure 23. A double-exponential function was the best model for each construct rate, which shows that there is a fast phase and a slow phase. The fast phase is defined as the timepoints up to 24 hrs, while the slow phase describes the degradation from 24 hrs to 96 hrs. The rate for each mutated construct in the beginning, k1 in Figure 23, is similar to the rate of wild-type $PahZ2_{KT-1}$. However, once the slow phase is reached, k2 in Figure 23, the mutated constructs have an increased rate compared to the wild-type, not just R165A. Once the NaCl was added, R162A and R162AR165A had a significant loss of activity as described previously.

5.4 Conclusion

The $PahZ2_{KT-1}$ substrate binding site relies on a trough of positively charged arginine residues to direct the polyanionic substrate toward the catalytic active site. All residues, with the exception of R162 and R165, contributed to a significant loss of activity when mutated to an alanine or glutamic acid, confirming their role in substrate binding. R162 showed similar catalytic activity to the wild-type, but was overwhelmed at lower concentrations by ionic interactions in the presence of salt. Residue R165 had similar total degradation to wild-type, and had an increased rate of degradation throughout all salt conditions. The data supports the prediction that the R165A residue was binding tightly to the substrate and decreased the number of substrate release events. When mutated to the neutral alanine or negatively charged glutamic acid, the residue was able to efficiently release the cleaved product, allowing for the rate of degradation to increase. Characterization of the substrate binding site helps with future engineering of the enzyme to reach the goal of cradle-to-cradle degradation of poly(aspartic acid).

CHAPTER 6

FUTURE RESEARCH: CHARACTERIZATION OF PAHZ1$_{KP-2}$

6.1 Introduction

PahZ1$_{KP-2}$ is an enzyme that was first isolated from the river water bacterial strain, *Pedobactor* sp. KP-2, and has specificity for β-linked PAA. The enzyme does function as a monomer, and site-directed mutagenesis has confirmed that PahZ1$_{KP-2}$ is a serine protease. While from a different species, there are overlapping structural characteristics when compared to PahZ1$_{KT-1}$. Future work aims to characterize PahZ1$_{KP-2}$, while comparing PAA degradation and structural differences with PahZ1$_{KT-1}$.

6.2 Methods

6.2.1 PahZ1$_{KP-2}$ Transformation, Expression and Purification

The gene for PahZ1$_{KP-2}$ was cloned in the pET15b vector with a 5' NdeI and 3' BamH1 restriction site. The synthesis and cloning of the plasmid was performed by GenScript (Piscataway, NJ), and an N-terminus 6X His tag was included for purification. The plasmid was transformed into BL21 (DE3) *E. coli* cells according to the NEB protocol (New England Biolabs, Ipswich, MA) with the following exceptions: 250 uL of SOC was added, no serial dilutions were performed, and 25 uL and 250 uL of transformed cells were spread onto 1.5% LB Agar selection plates with carbenicillin to incubate. A well isolated colony was selected to inoculate 50 mL of lysogeny broth (LB) media containing 50 µg/mL carbenicillin. The starter growth then incubated overnight at 37 ℃, shaking at 225 rpm. This growth was screened by purifying the plasmid according to the GeneJET Plasmid Miniprep Kit protocol (Thermo Scientific, Lithuania). PahZ1$_{KP-2}$ was incubated at 37 ℃ for 20 minutes with restriction endonucleases NdeI and BamHI for analysis using 1.2% Agarose gel electrophoresis.

Once screened for purity, 12.5 mL of the starter growth was used to inoculate 500 mL of LB-carb in 2L expression flasks. Cells were grown at 37 ℃, 225 rpm until the optical density (O.D.$_{600}$) reached a range of 0.6 – 0.8. Once the ideal O.D.$_{600}$ was reached, each flask was induced with 0.1 mM isopropyl β-

D-1-thiogalactopyranoside (IPTG, GoldBio, St. Louis, MO) and transferred to incubate at 20 ℃, 225 rpm overnight. Cells were harvested using centrifugation at 10,000 xg for 20 min at 4 ℃, and then stored at -20 ℃.

The harvested cells were resuspended in start buffer (50 mM Tris, pH 8.0, 300 mM NaCl, and 20 mM imidazole), and lysed by sonication in an ice bath over a 45 min cycle with a 20 sec pulse, 59 sec rest, and 58% amplification. Following lysis, 125 units/mL of turbonuclease (Accelagen, San Diego, CA) and 10 µg/mL of lysozyme were added to enhance bacterial cell wall breakdown and remove genomic DNA. The cell lysate was rocked for 60 min at room temperature, then centrifuged at 10,000 xg for 20 min at 4 ℃ to pellet cell debris. The supernatant was loaded onto an AKTA FPLC with a HisPur Ni-nitriloacetic acid (NiNTA) column (Thermo Scientific, Waltham, MA) equilibrated in start buffer. The $PahZ1_{KP\text{-}2}$ protein was eluted from the NiNTA column using elution buffer (50 mM Tris, pH 8.0, 300 mM NaCl, 500 mM imidazole) over 60 min using a 0-100% gradient. Fractions of 3 mL were collected and run on a 12.5% SDS-PAGE at 150 V to analyze purity and identify elution peak on the corresponding purification chromatogram. Identified fractions were collected and dialyzed in 20 mM Tris, pH 7.4, to get rid of any remaining imidazole. The purified protein was then stored on ice for characterization experiments.

6.2.2 GPC Activity Assays

To characterize the rate of substrate degradation, gel permeation chromatography (GPC) assays were performed with $PahZ1_{KP\text{-}2}$. The substrate, tPAA, was synthesized according to Andrzejak et al.[13], and 100 mg was solubilized in 1 mL of 50 mM sodium phosphate, pH 7.0, with 3 mg of internal standard, thyroglobulin (MilliporeSigma, Burlington, MA). Each sample contained 0.01 mg/mL of $PahZ1_{KP\text{-}2}$ and 24.5 µL of the substrate solution, with a final volume of 100 µL. Samples were incubated at 37 ℃ for the following amount of time; 10 min, 15 min, 20 min, 30 min, 45 min, 1 hr, 2 hr, 3 hr, and 4 hr. Each sample was heat precipitated at 70 ℃ for 10 mins after incubation with the substrate, then stored at -80 ℃ until loaded on the Shimadzu GPC.

To analyze degradation of the tPAA substrate over time, 10 µL of each sample was loaded onto a Shimadzu GPC with a Yarra 3 µM SEC-2000, 300 x 7.8 mm column (Phenomenex, Torrance, CA) equilibrated in 50 mM sodium phosphate, pH 7.0. Samples were detected by a refractive index detector, and the thyroglobulin was used as an internal standard to account for any differences in load amounts or any chromatographic shifts. The common oligomeric aspartic acid (OAA) product peak appeared at a retention time of 10.5 min, and a ratio of the product peak height compared to the internal standard height at a retention time of 5.0 min was used to calculate the total amount of tPAA degradation at each timepoint.

6.2.3 PahZ1$_{KP-2}$ Mutant Construct Analysis using GPC

The relative activity of PahZ1$_{KP-2}$ mutated constructs S126A, D194A, R215A, R215E, R215K, and F145H were determined by setting up a GPC assay using the same methods reported in Section 6.2.2., however, each construct only incubated for a single timepoint of 24 hrs. The formation of product for each mutant was compared to the wild-type at a retention time of 10.5 min, in which the wild-type was set as 100% product formation.

6.3 Results and Discussion

6.3.1 Overview of the PahZ1$_{KP-2}$ Crystal Structure

Recently, the crystal structure of PahZ1$_{KP-2}$ was determined, Figure 24A. The structure was previously predicted using AlphaFold software and closely aligns with the determined crystal structure of PahZ1$_{KT-1}$, shown in Figure 24B. Residue R215, analogous to the R246 residue identified in PahZ1$_{KP-2}$, seems to play a significant role in catalytic activity which shown in preliminary GPC activity assays. When the structure of PahZ1$_{KP-2}$ was aligned with the structure of PahZ1$_{KT-1}$, residue F145 in a non-conserved lipase box was identified in PahZ1$_{KP-2}$. This residue in PahZ1$_{KT-1}$ is a histidine near the catalytic active site, and construct F145H PahZ1$_{KP-2}$ was made to compare activity to further analyze the role of the residue.

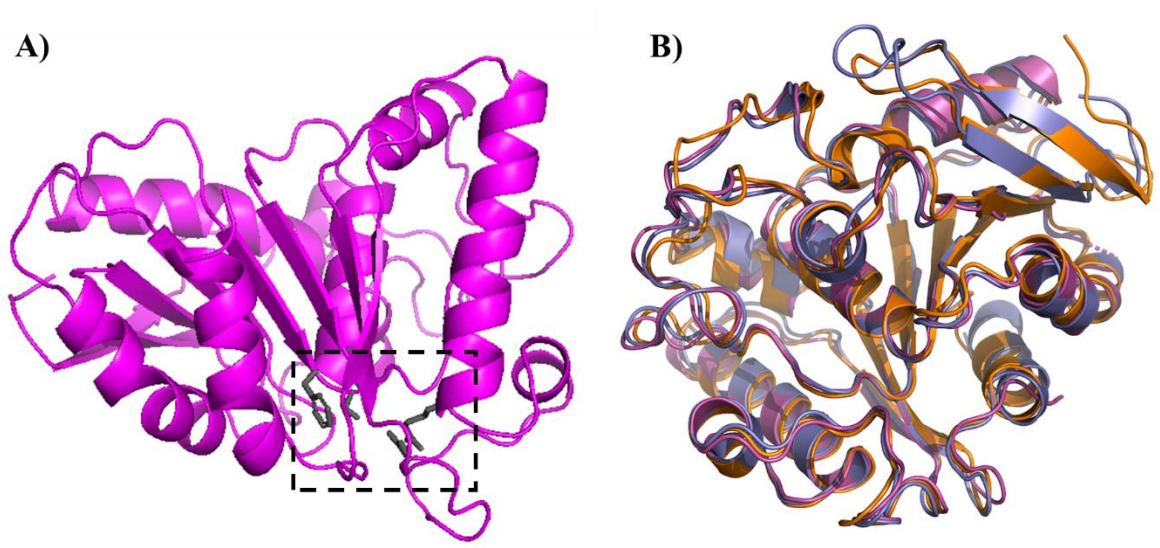

Figure 24. Cartoon representation of the PahZ1$_{KP-2}$ crystal structure. A) The cartoon representation shows the proposed crystal structure of PahZ1$_{KP-2}$. The enzyme is a monomer, with the catalytic active site highlighted by the dashed black box, with catalytic residues colored in gray. B) Superposition of PahZ1$_{KP-2}$ (magenta), PahZ1$_{KP-2}$ AlphaFold structure (slate), and PahZ1$_{KT-1}$ (orange).

6.3.2 Preliminary Catalytic Activity Data

GPC analysis was used to analyze the degradation of PAA after incubation with PahZ1$_{KP-2}$. First, the chromatogram was compared to the chromatogram of PahZ1$_{KT-1}$. Comparing the chromatograms, PahZ1$_{KP-2}$ forms a product that is larger than the product formed by PahZ1$_{KT-1}$. This size difference is identified by the difference in elution times, shown in Figure 25. The slight shift to the right

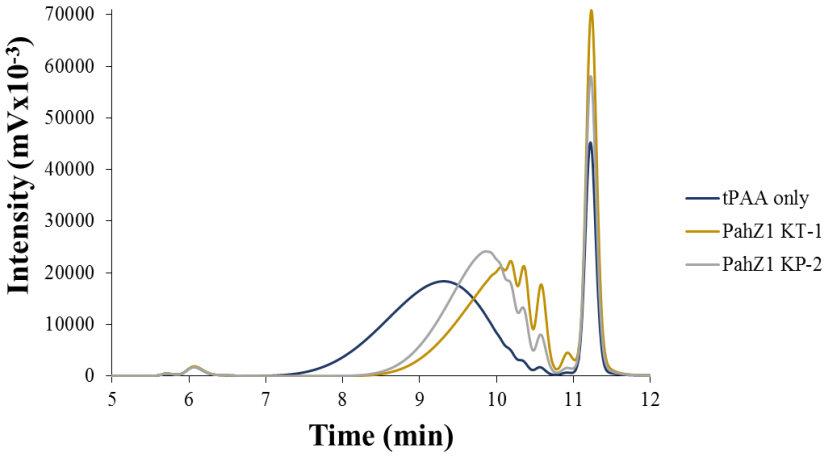

Figure 25. Representative GPC chromatogram of PahZ1$_{KP-2}$ and PahZ1$_{KT-1}$ PAA degradation. The tPAA control (blue) contains no enzyme, only tPAA and thyroglobulin as an internal standard. Each enzyme incubated for 24 hrs before heat precipitation to stop activity. PahZ1$_{KT-1}$ is shown in yellow, while PahZ1$_{KP-2}$ is shown in gray. As retention time increases, the size of the product decreases when using GPC. Thyroglobulin was added to each sample and is represented by the peak at a retention time of 6.0 minutes.

signifies a smaller product has been formed. Future work includes analysis of product molecular weight when comparing PahZ1$_{KT-1}$ and PahZ1$_{KP-2}$.

Further GPC analysis included rate analysis of tPAA degradation. The enzyme incubated with tPAA at various timepoints over a period of 4 hours, and the amount of product formed over time was calculated as percent relative activity. The relative activity was analyzed at a retention time of 7.75 minutes, which is where significant tPAA degradation was identified. The height of the peak at 7.75 minutes was divided by the peak height at 6.0 minutes, which was the internal standard peak. The ratio was used to determine the relative activity over 4 hours of time, Figure 26A.

Using the structure of PahZ1$_{KT-1}$, the catalytic residues for PahZ1$_{KP-2}$ were predicted and mutants S126A and D194A were made through site-directed mutagenesis. Constructs R215A, R215E, R215K, and F145H were also made. The catalytic activity of each construct was determined using GPC analysis after incubating with tPAA for 24 hours. The amount of product formed at a retention time of 10.55 minutes was compared to PahZ1$_{KP-2}$ wild-type, which was set as 100%. The results of this assay are shown in Figure 26B. The results confirm that S126, D194, and R215 are necessary for catalytic activity

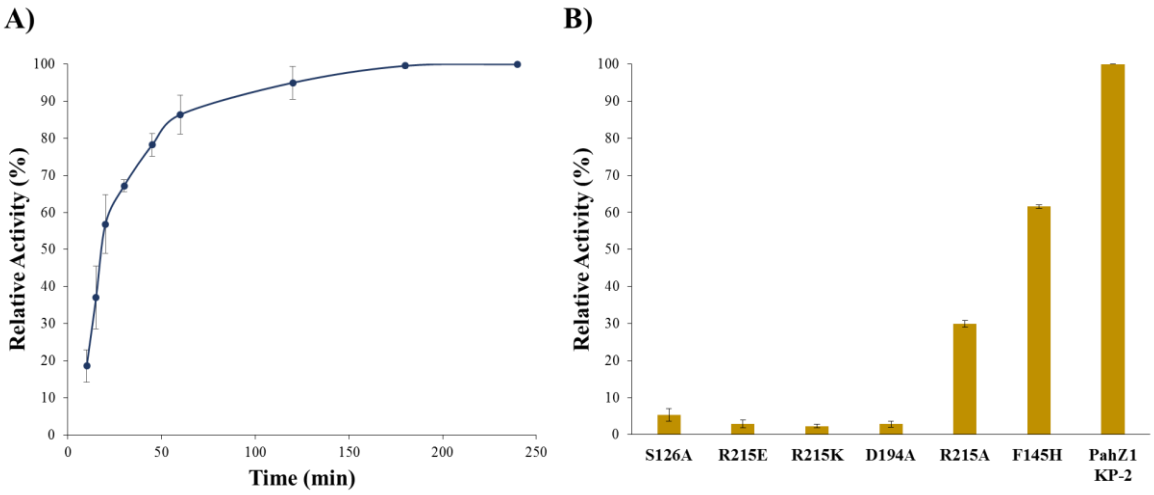

Figure 26. Relative activity of PahZ1$_{KP-2}$. A) The percent activity of wild-type PahZ1$_{KP-2}$ determined by analyzing the degradation of tPAA over a period of 4 hours. B) Relative activity of each mutated construct compared to wild-type. The error bars represent the standard deviation of triplicate measurements.

as each mutated construct had a significant loss of activity showing less than 6% product formed, with the exception of R215A. Construct R215A also had a significant loss of activity but retained about 30% activity compared to wild-type. The mutant that retained the most activity was F145H, which only had about 61.5% activity compared to the wild-type. The loss of activity when F145 was mutated to a histidine confirms that F145 is necessary for catalytic activity, however, molecular dynamic studies would help specify the role of the residue compared to the overlapping histidine in PahZ1$_{KT-1}$.

6.4 Conclusion

Preliminary data gives a lot of information about PahZ1$_{KP-2}$, but there is still data that should be collected to characterize the enzyme. While very similar to PahZ1$_{KT-1}$, analysis of product size needs to be performed using GPC. The slight chromatographic shift to the right indicates a smaller product is formed by PahZ1$_{KT-1}$, and quantitative analysis of molecular weight is necessary. Molecular dynamic studies would be helpful in characterizing the role of each mutated construct, as it was surprising that R215A had more activity than R215E or R215K. It was originally predicted that R215K would have more activity, as the lysine is similar in structure to the arginine it replaced, and was expected to function in a comparable manner due to the similarity in side chain length and charge. Molecular dynamic studies would also be helpful in understanding the role of F145, and why the relative activity decreased when mutated to a histidine. Due to the similarity between PahZ1$_{KT-1}$ and PahZ1$_{KP-2}$, further studies include introduction to chemical and heat denaturants, to determine if PahZ1$_{KP-2}$ retains activity in a similar manner to the monomeric PahZ1$_{KT-1}$ constructs.

CHAPTER 7

CONCLUSION

Consumer demand for products containing water-soluble polymers is not going to decline, instead, production is expected to increase by more than 5% over the next few years.[24] While biodegradability of a product is becoming more of a concern for consumers, that isn't enough to stop the constant accumulation of WSPs in the environment. Therefore, there is a need to come up with alternatives in which biodegradation can be enhanced or improved upon. With poly(aspartic acid) as an environmentally friendly WSP, characterization and improvement of the three enzymes responsible for its degradation are necessary to be able to complete a cradle-to-cradle process.

PahZ1$_{KT-1}$ was the first enzyme studied, and initial efforts focused on obtaining a pure protein product. After successful transformation, expression, and purification, the pure protein was used in crystallization experiments and activity assays. Crystallization experiments led to the determination of the crystal structure, in which PahZ1$_{KT-1}$ was identified as a dimer made up of two monomeric units with two-fold rotational symmetry along the interface. It was determined that PahZ1$_{KT-1}$ is a serine protease, which was further confirmed through GPC activity analysis of constructs with mutations introduced at the catalytic active site, S157A and D225A. R246 was identified as a residue necessary for catalytic activity and is predicted to be responsible for the β-linked tPAA specificity exhibited by PahZ1$_{KT-1}$. The importance of this residue was also confirmed through GPC analysis of mutated constructs R246A, R246E and R246K. Once the residues necessary for catalytic activity had been identified, efforts shifted toward determining the necessity of the dimeric structure.

Initial characterization of PahZ1$_{KT-1}$ led to the identification of residues responsible for ionic interactions along the dimeric interface. Attempts were made to first disrupt the interface with the introduction of salt, but SEC analysis showed that salt did not disrupt the dimer. Site-directed mutagenesis was then used to create two different constructs with mutations along the interface, E251K and IM. Once constructs E251K and IM had been successfully transformed, expressed, and purified, the purified protein was used in a variety of studies. The first experiment used SEC to confirm that the

mutations had in fact disrupted the ability of the enzyme to form a dimer, and the data was further supported by DLS experiments. Once it was confirmed that constructs E251K and IM were monomers, GPC activity analysis was used to determine if the monomer retained catalytic activity. Compared to the wild-type, there was no difference in tPAA degradation over a four hour period between the dimer and monomeric constructs. The next step was to determine if the dimer was more stable than the monomers when introduced to chemical or heat stress. The introduction of a chemical denaturant showed no difference in catalytic activity with E251K and the IM, while the wild-type had a loss of activity. Similar results were seen with the heat precipitation studies. The melting temperature of each was calculated using UV-Vis spectroscopy to determine if there was a difference in stability between wild-type PahZ1$_{KT-1}$, IM, and E251K. Melting temperatures for each construct were not significantly different between the monomer and dimer. Further analysis of refolding after chemical denaturation did not show a significant difference in recovery, however the wild-type did have the highest percent recovered. After, after heat precipitation, wild-type had the lowest recovery percentage (73.5 ± 9.3%) while E251K had the most amount of protein recovered (89.5 ± 4.3%).

While the data was similar without chemical denaturation or heat precipitation, there was a difference in recovery and retention of catalytic activity after introduction to stressors. Constructs E251K and IM retained more catalytic activity during GPC analysis, suggesting that they had refolded properly compared to wild-type, which had a loss of activity. While wild-type PahZ1$_{KT-1}$ may take more energy to denature and therefore refold, the monomeric constructs seemed to fold and retain catalytic activity more efficiently which is important from an industrial perspective.

While working to improve PahZ1$_{KT-1}$, efforts were also focused on characterizing the second enzyme, PahZ2$_{KT-1}$. Initial efforts were the same as with PahZ1$_{KT-1}$, and the pure protein products of PahZ2$_{KT-1}$ were used to determine the crystal structure and characterize the activity of the enzyme. With the crystal structure identified, PahZ2$_{KT-1}$ is defined as an M28 metalloprotease. Made up of a dimeric and catalytic domain, a bound metal ion is necessary at the active site for the retention of catalytic activity. Through GPC activity assays, zinc was identified as the ideal metal, a result that was supported by

molecular modeling studies as the zinc ions form the preferred tetrahedral geometry. Mutations along the catalytic active site, specifically mutations along both zinc binding sites, were introduced to confirm the necessity of two metal ions for activity as well as to confirm the role of each residue at the zinc binding sites. GPC activity analysis showed a significant loss of activity with the mutations, and confirmed the necessity of both zinc ions. GPC analysis also showed an increased rate of degradation in the presence of salt and a conformational change along the hinge region was identified. Molecular dynamic studies identified residues that were predicted to be necessary for substrate binding and further analysis of the substrate binding site was performed by creating multiple mutated constructs.

Mutations introduced along the substrate binding site confirmed the role of each residue. GPC analysis showed a significant decrease in activity when residues R200, R270, and R316 were mutated, confirming their necessary role along the dimeric domain for substrate orientation and catalytic activity. When residues R162 and R165 were mutated, there was an increased rate of degradation seen. While the enhanced rate was not seen with R162A or R162AR165A in the presence of salt, R165A did retain its increased rate of degradation compared to the wild-type. Understanding the role each residue plays along the substrate binding site is necessary for improving the efficiency of the enzyme as well as for engineering an enzyme that can break down more than just poly(aspartic acid).

Future efforts include the characterization of the third enzyme, $PahZ1_{KP-2}$. While this enzyme is from a different bacterial strain, it is very similar in structure to $PahZ1_{KT-1}$. The crystal structure of this enzyme has been determined, and preliminary data has identified residues that are likely apart of the catalytic active site or necessary for catalytic activity.

Structure determination and characterization of each protein brings the reality of a cradle-to-cradle degradation process even closer. Protein engineering can be used to continue to improve each enzyme, as well as modify the enzymes to break down a variety of WSPs, not just poly(aspartic acid). The amount of WSPs in the environment is going to continue to increase, and it is important to not only try to find biodegradable alternatives, but to find ways to improve the degradation so that products can be broken down to components that can be reused in a sustainable manner.

REFERENCES:

1. Billiet, S.; Trenor, S. R., 100th Anniversary of Macromolecular Science Viewpoint: Needs for Plastics Packaging Circularity. *ACS Macro Letters* **2020,** *9* (9), 1376-1390.

2. Chen, Y.; Awasthi, A. K.; Wei, F.; Tan, Q.; Li, J., Single-use plastics: Production, usage, disposal, and adverse impacts. *Sci Total Environ* **2021,** *752*, 141772.

3. Arp, H. P. H.; Knutsen, H., Could We Spare a Moment of the Spotlight for Persistent, Water-Soluble Polymers? *Environ Sci Technol* **2020,** *54* (1), 3-5.

4. Huppertsberg, S.; Zahn, D.; Pauelsen, F.; Reemtsma, T.; Knepper, T. P., Making waves: Water-soluble polymers in the aquatic environment: An overlooked class of synthetic polymers? *Water Res* **2020,** *181*, 115931.

5. Nisticò, R., Polyethylene terephthalate (PET) in the packaging industry. *Polymer Testing* **2020,** *90*, 106707.

6. Austin, H. P.; Allen, M. D.; Donohoe, B. S.; Rorrer, N. A.; Kearns, F. L.; Silveira, R. L.; Pollard, B. C.; Dominick, G.; Duman, R.; El Omari, K.; Mykhaylyk, V.; Wagner, A.; Michener, W. E.; Amore, A.; Skaf, M. S.; Crowley, M. F.; Thorne, A. W.; Johnson, C. W.; Woodcock, H. L.; McGeehan, J. E.; Beckham, G. T., Characterization and engineering of a plastic-degrading aromatic polyesterase. *Proc Natl Acad Sci* **2018,** *115* (19), E4350-E4357.

7. Jop, K. M.; Guiney, P. D.; Christensen, K. P.; Silberhorn, E. M., Environmental fate assessment of two synthetic polycarboxylate polymers. *Ecotoxicol Environ Saf* **1997,** *37* (3), 229-37.

8. Hennecke, D.; Bauer, A.; Herrchen, M.; Wischerhoff, E.; Gores, F., Cationic polyacrylamide copolymers (PAMs): environmental half life determination in sludge-treated soil. *Enviro Sci Europe* **2018,** *30* (1), 16.

9. Xiong, B.; Loss, R. D.; Shields, D.; Pawlik, T.; Hochreiter, R.; Zydney, A. L.; Kumar, M., Polyacrylamide degradation and its implications in environmental systems. *npj Clean Water* **2018,** *1* (1), 17.

10. Xu, W.; Tan, L.; Zhao, T.; Zhu, X.; Wang, J., Toxicity assessments of acrylamide in aquatic environment using two algae Nitzschia closterium and Scenedesmus quadricauda. *Enviro Sci and Pollut Research* **2020,** *27* (16), 20545-20553.

11. Jop, K. M.; Guiney, P. D.; Christensen, K. P.; Silberhorn, E. M., Environmental Fate Assessment of Two Synthetic Polycarboxylate Polymers. *Ecotoxicol Environ Saf* **1997,** *37* (3), 229-237.

12. Thombre, S. M.; Sarwade, B. D., Synthesis and Biodegradability of Polyaspartic Acid: A Critical Review. *J. Macromol. Sci, Part A* **2005,** *42* (9), 1299-1315.

13. Andrzejak, S.; Moyer, S.; Quillian, B.; Shank, N., Revisiting a Green Polymerization of Aspartic Acid for a Second-Semester Introductory Organic Chemistry Laboratory: Improvements, Learning Objectives, and Post-Laboratory Assignment. *Chem Educ* **2018,** *23*.

14. Hiraishi, T.; Maeda, M., Poly(aspartate) hydrolases: biochemical properties and applications. *Appl Microbiol Biotechnol* **2011,** *91*, 895+.

15. Matsubara, K.; Nakato, T.; Tomida, M., End Group and Irregular Structure Analysis in Thermally Prepared Sodium Polyaspartate by 1H and 13C NMR Spectroscopy. *Macromolecules* **1998,** *31* (5), 1466-1472.

16. Tabata, K.; Abe, H.; Doi, Y., Microbial Degradation of Poly(aspartic acid) by Two Isolated Strains of Pedobacter sp. and Sphingomonas sp. *Biomacromolecules* **2000,** *1* (2), 157-161.

17. Tabata, K.; Kajiyama, M.; Hiraishi, T.; Abe, H.; Yamato, I.; Doi, Y., Purification and characterization of poly(aspartic acid) hydrolase from Sphingomonas sp. KT-1. *Biomacromolecules* **2001,** *2* (4), 1155-60.

18. Hiraishi, T.; Kajiyama, M.; Yamato, I.; Doi, Y., Enzymatic hydrolysis of alpha- and beta-oligo(L-aspartic acid)s by poly(aspartic acid) hydrolases-1 and 2 from Sphingomonas sp. KT-1. *Macromol Biosci* **2004,** *4* (3), 330-9.

19. Weiland, M. H., Enzymatic Biodegradation by Exploring the Rational Protein Engineering of the Polyethylene Terephthalate Hydrolyzing Enzyme PETase from *Ideonella sakaiensis* 201-F6. In *Mechanistic Enzymology: Bridging Structure and Function*, American Chemical Society: **2020**; Vol. 1357, pp 161-174.

20. Brambley, C. A.; Bolay, A. L.; Salvo, H.; Jansch, A. L.; Yared, T. J.; Miller, J. M.; Wallen, J. R.; Weiland, M. H., Structural Characterization of Sphingomonas sp. KT-1 PahZ1-Catalyzed Biodegradation of Thermally Synthesized Poly(aspartic acid). *ACS Sus Chem & Eng* **2020,** *8* (29), 10702-10713.

21. Lamantia, T.; Jansch, A.; Marsee, J. D.; Weiland, M. H.; Miller, J. M., Engineered Sphingomonas sp. KT-1 PahZ1 monomers efficiently degrade poly(aspartic acid). *Biophysical Chem* **2022,** *281*, 106745.

22. Hiraishi, T.; Kajiyama, M.; Tabata, K.; Abe, H.; Yamato, I.; Doi, Y., Biochemical and molecular characterization of poly(aspartic acid) hydrolase-2 from sphingomonas sp. KT-1. *Biomacromolecules* **2003,** *4* (5), 1285-92.

23. Brambley, C. A.; Yared, T. J.; Gonzalez, M.; Jansch, A. L.; Wallen, J. R.; Weiland, M. H.; Miller, J. M., Sphingomonas sp. KT-1 PahZ2 Structure Reveals a Role for Conformational Dynamics in Peptide Bond Hydrolysis. *J Phys Chem B* **2021,** *125* (22), 5722-5739.

24. Vandermeulen, G. W. M.; Boarino, A.; Klok, H.-A., Biodegradation of water-soluble and water-dispersible polymers for agricultural, consumer, and industrial applications—Challenges and opportunities for sustainable materials solutions. *J Polymer Sci* **2022,** *n/a* (n/a).